9

All-Optical Pulse Shaping in the Sub-Picosecond Regime Based on Fiber Grating Devices

María R. Fernández-Ruiz,[1] Alejandro Carballar,[2] Reza Ashrafi,[1,3] Sophie LaRochelle,[4] and José Azaña[1]

[1] *Energy, Materials & Telecommunications Research Centre, INRS, Montreal, Quebec, Canada*
[2] *Department of Electronic Engineering, University of Seville, Seville, Spain*
[3] *Department of Electrical and Computer Engineering, McGill University, Montreal, Quebec, Canada*
[4] *Center for Optics, Photonics and Lasers, Laval University, Quebec, Canada*

9.1 Introduction

Optical pulse shaping involves synthesizing the desired shape of the complex (amplitude and phase) temporal envelope of an optical electromagnetic wave, and it plays a fundamental role in communication and computation systems. Pulse shaping techniques are required to generate advanced pulse waveforms that optimize the overall performance of a communication system, e.g., with the aim of extending the transmission reach of the communication link, achieving optical multiplexing at highest spectral efficiency, or limiting nonlinear distortions. Optical pulse shapers are also important building blocks to implement specific source or channel encoding strategies. Moreover, pulse shaping has been also employed for the generation of optimized control signals in nonlinear-based signal processing blocks, aimed at switching and routing of information in the optical domain.

In order to generate a particular optical pulse form, one needs to be able to reliably define the amplitude and phase profile of an optical field. Typically, the pulsed laser sources generate a train of transform-limited pulses with a Gaussian-like complex envelope. However, for some applications it is necessary to modify the shape of these pulses, i.e., their amplitude and/or phase profiles. Examples of desired optical shapes for optical signal processing applications are the following:

1. *Flat-top (rectangular) shape:* One of its main applications is their use in nonlinear optical switching, most prominently in the context of temporal de-multiplexing of optical time-division multiplexing (OTDM) systems [1, 2]. The approximately constant intensity of flat-top pulses defines a clean switching time window avoiding the problem of pulse breakup, which is a main reason of degradation in the

Shaping Light in Nonlinear Optical Fibers, First Edition. Edited by Sonia Boscolo and Christophe Finot.

performance of optical temporal switches [3]. Another application of rectangular pulses is wavelength conversion by optical time gating, where they are employed as pump pulses. The duration of the gate opening time depends on the pump pulse width and the wavelength tunability depends on their pump pulse power [4]. Additionally, flat-top pulses are required on orthogonal frequency division multiplexing (OFDM), where the system data is encoded onto subcarriers with a rectangular shaped impulse response [5].

2. *Parabolic shape:* Parabolic pulses are of interest to achieve ultra-flat self-phase modulation (SPM)-induced spectral broadening in super continuum generation experiments [5, 6]. They are also attractive for nonlinear signal processing methods based on the use of linearly chirped pump pulses, such as for implementation of nonlinear pulse retiming or time-lens processes [7, 8].
3. *Triangular or saw-tooth pulses:* These are widely employed for several applications, such as the implementation of tunable delay lines, time-domain add-drop multiplexing, wavelength conversion, doubling of optical signals, time-to-frequency mapping of multiplexed signals, etc. [6, 9].
4. *Sinc-shape:* They are of high interest for orthogonal time division multiplexing, where the symbols are transmitted by Nyquist pulses (i.e., Nyquist pulse shaping) [10, 11].
5. *High-order modulation codes:* The generation of fixed several-symbol codes using high-order modulation formats is particularly of interest for optical code-division multiple access (OCDMA) and optical-label-switching communications [12].

9.2 Non-Fiber-Grating-Based Optical Pulse Shaping Techniques

A straightforward method for shaping optical waveforms involves the use of high-speed electronics to directly drive an external electro-optical modulator (EOM). The modulating signal is an electronic waveform with the targeted shape that carves the information in an optical carrier [13, 14]. The speed limitation of the electronics typically limits the generated optical waveforms to frequency contents below a few tens of GHz.

Pulse shaping methods based on Fourier optics are well known and have been widely applied. These methods, also referred to as "spectral shaping," routinely offer temporal resolutions better than 100 fs. In the original technique, the temporal information is converted into a one-dimensional spatial domain waveform through a diffraction grating. The resulting waveform is shaped by a simple linear filtering process based on the concatenation of two Fourier-transform systems in a configuration called 4-f_l system, with f_l being the focal length of the involved thin lens. In the central plane of the system, the so-called Fourier plane, an amplitude or phase mask is placed, which acts as the optical filter implementing modulation of the different spatial frequency components of the input beam, as depicted in Figure 9.1. The resulting shaped wave is converted back to the time-domain via a second diffraction grating. To date, conventional picosecond and femtosecond pulse shaping techniques have been implemented by replacing the amplitude or phase mask by advanced devices, such as liquid crystal spatial light modulators [15–17], acousto-optic modulators [15], or electro-optical phase arrays [17], that impart user-specified spectral amplitude and phase modulations on the pulse in a programmable fashion.

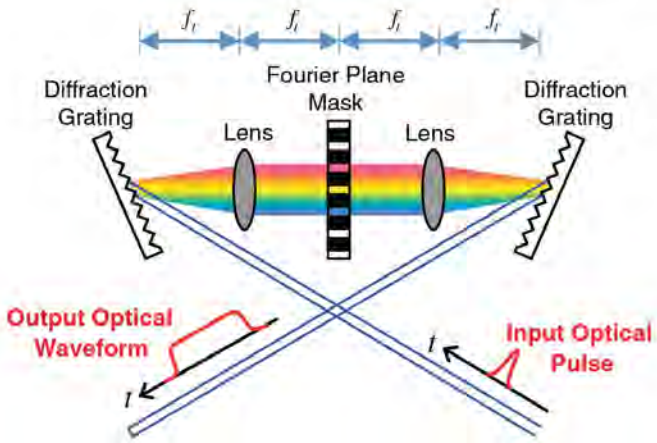

Figure 9.1 Optical arbitrary waveform generation by means of a spatial-domain pulse shaper. The output waveform is determined by the Fourier transform of the pattern transferred from the spatial mask onto the input waveform spectrum.

The main drawback of Fourier-optics-based pulse shaping methods is the need for bulky optical components, which require strict tolerances in their alignment and have limited integration with waveguide devices. Also, the need to couple the shaped waveforms back into a single-mode fiber (SMF) introduces loss and further limits the temporal extent of the generated pulse shapes [18]. To overcome this practical complexity problem, an important body of research has focused on the search for alternative implementations of spectral shaping using optical fiber or integrated-waveguide platforms.

To give a first relevant example, an integrated version of the original Fourier-optics pulse shaping concept has been implemented using arrayed waveguide gratings (AWGs), which have been used to spatially distribute the temporal frequency components of an input waveform. The amplitude and phase profile of the spatially-dispersed pulse is subsequently manipulated with an array of modulators and combined again using a second AWG [19, 20]. AWG-based pulse shapers are compact, integrated devices, but they are typically limited to time resolutions above 10 ps.

A pulse shaping approach similar to the previous one has recently been developed [21]. However, in this case, the employed input signal is an optical frequency comb (OFC). Each line of the OFC is separately modulated using in-phase and quadrature-phase (IQ) modulators and then, the spectral slices are combined to produce a target waveform. This technique is able to generate broad bandwidth signals (scalable to THz frequencies) from narrow spectral slices with bandwidths accessible by current electronics. However, the complexity, cost and power consumption of the required electronic circuits quickly scale up with the bandwidth of the output signal.

With an understanding of the space-time duality (mathematical equivalence between free-space diffraction and narrowband temporal dispersion [22]), the equivalent of pulse-shapers based on spatial-domain optical filtering has been implemented using in-line fiber-optics components. In particular, the spatial 4-f_f system can be substituted by two all-fiber dispersive elements with opposite dispersion and a single EOM in between the dispersive elements. This implementation based on pure fiber optics offers the advantages of smaller size, lower loss, better stability and higher potential for integration [18]. Different schemes have been proposed based on this configuration, using

either an electro-optical intensity modulator [23, 24] or a phase modulator [25–27], all of them with a resolution reaching the sub-picosecond range.

All the previously mentioned approaches, essentially based on Fourier optics, are programmable, as the filter spectral response is generally generated through an electrical bit pattern generator or arbitrary waveform generator.

Simpler, more compact optical pulse shapers have been also explored using fiber-optics or integrated-waveguide linear optical filters with customized spectral responses. A relevant example is that of optical lattice filters [28–30]. They are a good all-purpose solution due to their ability to generate complicated spectral transfer functions by cascading identical units cells. In a widely used configuration each unit cell employs a combination of a ring resonator and a Mach-Zehnder interferometer, and it contributes a separately controllable pole and zero pair [30]. However, the requirement of a phase-shifter as part of the interferometer in each unit cell makes it difficult to achieve operation bandwidths above a few GHz.

Alternative pulse shaping techniques have been also demonstrated using the concept of temporal coherence synthesization. They are based on the synthesis of the desired output pulse shape by coherently combining a set of input pulse replicas with different time delays [31]; or similarly, using coherent overlapping of different (first and high-order) derivatives of the input optical pulse with specific relative weights [32]. Programmability can be achieved by properly programming the time-delays (first approach) or relative weights using amplitude and/or phase optical modulators (second approach).

Finally, another category of pulse shapers includes nonlinear elements that allow the controlled generation of frequency components outside the frequency spectrum of the input pulse-form. A comprehensive revision of nonlinear pulse shaping approaches can be found in the Chapter 5 of the present book. Nonlinear optical signal-processing devices enable all-optical operations at ultrahigh speeds, i.e., in the femtosecond regime. However, the current level of technological maturity of pulse shaping methods based on nonlinear effects, together with the high degree of control required on the specifications of the input pulse, e.g., power, central frequency, state of polarization, etc., translate into critical drawbacks for their application in practical, real-world systems. In general, optical pulse shaping based on optical nonlinearities is not energy-efficient, high optical powers are commonly required and for now, the pulse shaping operation is limited to a few intensity-only optical shapes [33, 34].

9.3 Motivation of Fiber-Grating Based Optical Pulse Shaping

Fiber gratings are periodic perturbations of the refractive index along the core of an optical fiber, typically generated by the exposition of an optical fiber to a spatially varying pattern of ultraviolet light. Since their discovery in 1978, fiber gratings have been extensively studied for their application as linear passive filters, with interesting advantages such a relatively low cost, low losses, polarization insensitivity and full compatibility with fiber-optics systems [35,36]. The main advantage of fiber gratings is their flexibility to implement nearly any desired linear optical filtering functionality, only constrained by practical fabrication limitations. Mathematically, the perturbation of the effective refractive index of the guided mode of interest along the fiber length z is described as

$$n_{FG}(z) = n_{eff} + \Delta n(z) \cdot \cos\left\{ \int_0^z \frac{2\pi}{\Lambda(z')} dz' \right\}, \tag{9.1}$$

where $\Delta n(z)$ is the envelope of the induced refractive index change, also defined as the apodization profile, and $\Lambda(z)$ is the period variation along the grating length.

Several theories have been used to model and describe the functionality of fiber gratings, but the most widely extended is the Coupled Mode theory [37,38]. This theory considers the fiber grating as a device able to couple optical power between two modes (with propagation constants, β_1 and β_2) when the grating period verifies the phase-matching condition [35]

$$\beta_1 - \beta_2 = m\frac{2\pi}{\Lambda}; \quad m = 1, 2, 3, \ldots \tag{9.2}$$

being m the Bragg-order. Hence, fiber gratings can be broadly classified into two types:

- *Fiber Bragg gratings* (FBGs, also called short-period gratings), which typically have a sub-micron period and act to couple light from the forward-propagating fundamental core-mode to the counter-propagating (backward) core-mode of the optical fiber, i.e, $\beta_2 = -\beta_1$. Single-mode operation is typically assumed. This coupling dominates at a specific wavelength, defined by the Bragg phase-matching condition (Eq. (9.2) considering $m = 1$). FBGs operate as a band-pass filter in reflection and, consequently, as band-stop filter in transmission (Figure 9.2).
- *Long period gratings* (LPGs), which have a period typically in the range of 100s of μm, and induce coupling between the propagating fundamental core-mode and higher-order cladding-modes (Figure 9.3). In LPGs, phase matching occurs at discrete wavelengths determined by the phase matching condition so the wavelength-dependent attenuation resonances occur at a range of different wavelengths, associated with the excitation of different specific higher-order cladding modes [35].

As linear, passive filters, fiber gratings have the properties of linearity and time invariance (LTI). Therefore, their functionality can be described using techniques based on Fourier transform analysis [39]. FBGs can then be characterized in both reflection and

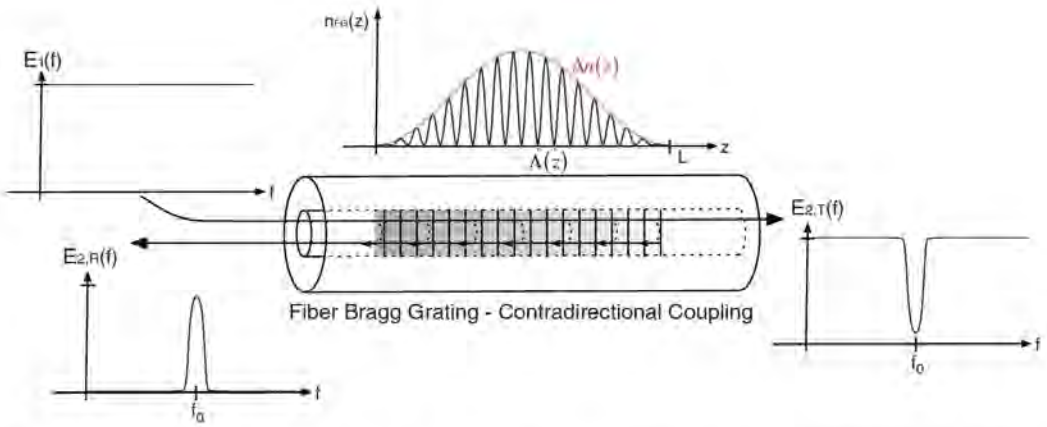

Figure 9.2 Schematic diagram of a fiber Bragg grating (FBG), indicating two operation possibilities: the reflection mode and the transmission mode.

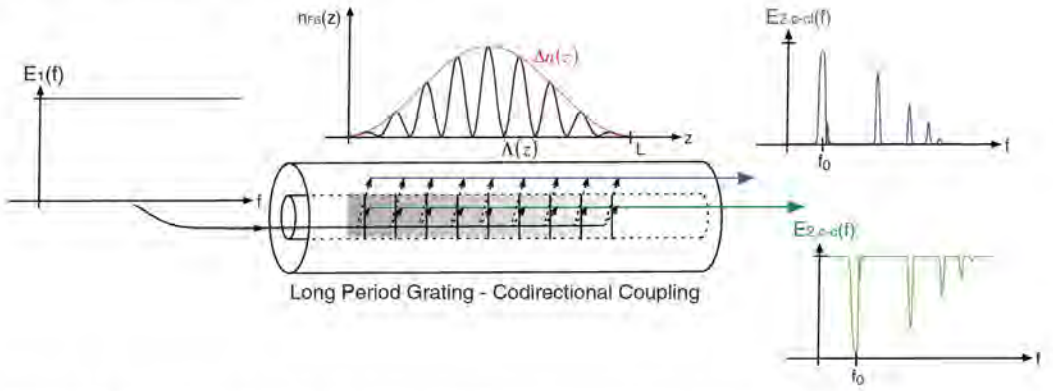

Figure 9.3 Schematic diagram of a long-period fiber grating (LPG), indicating two operation possibilities: the core-to-core mode and the core-to-cladding mode.

transmission operation by their frequency responses, $H_R(f)$ and $H_T(f)$, i.e., the spectral transfer function, or the corresponding temporal impulse responses, $h_R(t)$ and $h_T(t)$):

$$H_R(f) = \frac{E_{2,R}(f)}{E_1(f)}; \quad h_R(t) = \mathcal{F}^{-1}[H_R(f)]; \tag{9.3}$$

$$H_T(f) = \frac{E_{2,T}(f)}{E_1(f)}; \quad h_T(t) = \mathcal{F}^{-1}[H_T(f)], \tag{9.4}$$

where $\mathcal{F}$ denotes Fourier transformation, t is the time variable, and $f = f_{opt} - f_0$, with f_{opt} being the optical frequency variable and f_0 being the carrier frequency.

On the other hand, LPGs work in transmission offering two possibilities: the core-to-cladding coupling mode or core-to-core coupling, where single-mode operation is typically assumed in the fiber as well. For LTI analysis, it is assumed that the grating is operated over a relatively limited bandwidth around one of its resonance wavelengths so that one can assume that the coupling mainly occurs between the core mode and the single cladding mode corresponding to the relevant spectral resonance. Under this assumption, similarly to FBGs, the analogous spectral transfer functions and temporal impulse responses for the two interacting LPG modes are obtained as:

$$H_{c-cl}(f) = \frac{E_{2,c-cl}(f)}{E_1(f)}; \quad h_{c-cl}(t) = \mathcal{F}^{-1}[H_{c-cl}(f)]; \tag{9.5}$$

$$H_{c-c}(f) = \frac{E_{2,c-c}(f)}{E_1(f)}; \quad h_{c-c}(t) = \mathcal{F}^{-1}[H_{c-c}(f)]. \tag{9.6}$$

Let us assume an input optical waveform analytically defined as $e_1(t) = x(t) \cdot \exp(j2\pi f_0 t)$, where $x(t)$ is the input waveform's complex envelope and f_0 is the optical carrier frequency. By launching this optical waveform at the input of a fiber grating-based pulse shaper with a well-defined response around f_0, the output optical waveform can be expressed as $e_2(t) = y(t) \cdot \exp(j2\pi f_0 t)$. In this expression, $y(t)$ is the output waveform's complex envelope and it can be mathematically obtained as:

$$y(t) = h(t) * x(t); \tag{9.7}$$

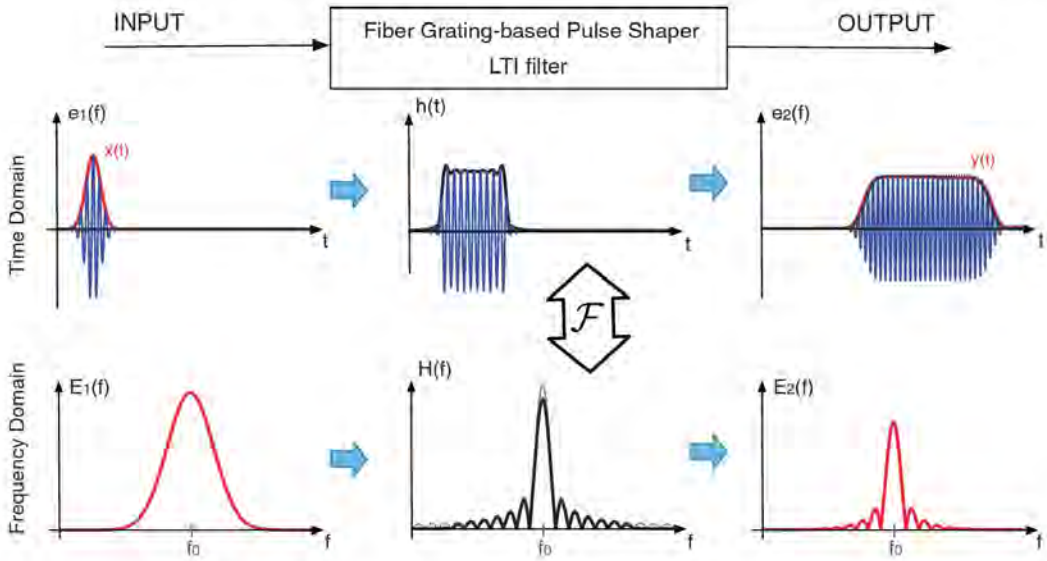

Figure 9.4 Schematic diagram for the operation principle of a fiber grating-based pulse shaper in the time and frequency domain.

where $h(t)$ is the filter's impulse response complex envelope (at f_0) and $*$ denotes the convolution operation. By applying the Fourier transform to Eq. (9.7), we then have:

$$Y(f) = H(f) \cdot X(f) \tag{9.8}$$

where $X(f)$, $Y(f)$ and $H(f)$ are the Fourier transforms of $x(t)$, $y(t)$ and $h(t)$, respectively. The frequency transfer function $H(f)$, or correspondingly the temporal impulse response $h(t)$, of the fiber grating can be designed to generate a target output complex envelop $y(t)$, within the frequency-bandwidth and time-window limitations of the linear filtering device, as depicted in Figure 9.4.

To design the targeted pulse shaper, both the spectral response of the input signal $X(f)$ and the desired output signal $Y(f)$ must be specified. As with any LTI filter, the transfer function of the pulse shaper is obtained as $H(f) = Y(f)/X(f)$. In order to achieve the targeted grating spectral response, nearly all the grating physical parameters can be varied: induced index change $\Delta n(z)$, length L, period chirp $\Lambda(z)$, and whether the grating supports counterpropagating or copropagating coupling at a desired frequency [35]. Intensive research has been carried out to develop design tools that provide a direct relationship between the refractive index perturbation and the resulting grating spectral response. Thus, analysis tools [35–38], i.e., tools that provide the grating spectral response $H(f)$ from the refractive index profile $n_{FG}(z)$; and synthesis tools, i.e., tools that provide the required $n_{FG}(z)$ from a targeted $H(f)$, have been developed and they nowadays possess a high level of technical maturity [40–43].

The performance of the fiber grating-based pulse shapers is typically characterized by two parameters: the time-bandwidth product (TBP) and the energy efficiency. The TBP

is obtained from the measurement of the cross-correlation coefficient, C_C between the actual, $y(t)$, and the ideal, $y_{ideal}(t)$, output waveforms. It can be obtained by:

$$C_C[\%] = \frac{\int_{-\infty}^{+\infty} y(t) \cdot y_{ideal}(t) \cdot dt}{\sqrt{\int_{-\infty}^{+\infty} y^2(t)dt \cdot \int_{-\infty}^{+\infty} y_{ideal}^2(t)dt}} \times 100\% \tag{9.9}$$

The TBP is calculated as the ratio between the maximum and the minimum temporal full-width at half maximum (FWHM) of an input Gaussian pulse for which the C_C is higher than a predefined value, e.g., 90% (corresponding to the ratio between the maximum and minimum 3dB-bandwidth of an input Gaussian pulse for which the C_C holds higher than the predefined value). On the other hand, the energy efficiency is defined as the output-to-input pulse energy ratio.

An important limitation of fiber grating solutions in their application as pulse shapers is the lack of reconfigurability. Fortunately, there are a broad range of applications for which a particular fixed temporal shape is required, e.g., rectangular or parabolic pulses. In those cases, a simpler, high efficient and easily reproducible component would be highly recommended over the schemes presented in Section 9.2. Some interesting pulse shaping components have been proposed and demonstrated simply based on passive linear filters, such as FBG or LPG [7,9,44–79]. Moreover, intense study is being done to be able to integrate these periodic structures on photonics integrated chips (PICs) [80–86].

9.3.1 Fiber Bragg Gratings (FBGs)

FBG is a fundamental component for many applications in fiber-optic communications, which has been extensively used and studied for a very wide range of applications based on linear optical filtering [7,9,44–74]. The fundamental advantage of FBGs is their flexibility to achieve almost any arbitrary spectral/temporal responses for optical pulse shaping when operating in reflection [35, 36].

9.3.1.1 Fiber Bragg Gratings Operating in Reflection

The more direct approach of use of an FBG as a frequency-filtering stage for pulse shaping applications consists of operating the grating in reflection within the limit of the first-order Born approximation (weak-coupling condition) [7, 9, 44–47]. Accordingly, if the grating is sufficiently weak, then the corresponding reflection impulse response $h_R(t)$ is directly related to the spatial profile of the index-modulation depth $\Delta n(z)$. This simple approach permits the synthesis of nearly any desired optical waveform with resolutions in the picosecond regime. As relevant examples of this design approach, we can mention the implementation of flat-top [45, 46], parabolic [7] and saw-tooth (triangular) [9] pulse shapers based on superstructured FBGs. However, working within the constraints of the Born approximation limits the maximum duration of the temporal waveforms that can be synthesized. In particular, for gratings that are longer than a few centimeters (this corresponds to temporal durations of the order of hundreds of picoseconds), the approach starts to fail even for very weak index modulations. The reason is that the Born approximation is strictly valid when $\kappa L \ll 1$, where κ is the coupling coefficient, related to the index modulation depth as $\kappa = \pi\Delta n/\lambda$ (λ is the wavelength, $\lambda = c_0/f$, with c_0 being the speed of light in vacuum). When the grating is too

long, the required Δn may be too weak to ensure light penetrates the full length so that the whole grating contributes identically to the reflected signal, challenging its practical realization.

Another approach for FBG-based pulse shaping based on the Born approximation was proposed to overcome the limitation in the duration of the output pulses of the previous method. The technique is based on a space-to-frequency-to-time mapping [48], and it enables the synthesis of arbitrary waveforms in the picosecond/nanosecond regime, although with a lower energy efficiency. This method consists of using a specially designed apodized linearly chirped FBG, in the regime of weak coupling condition. If the FBG chirp-induced dispersion $\ddot{\Phi}$ (s^2) is sufficiently large so that $\ddot{\Phi} \gg \Delta t_1^2/4$, with Δt_1 being the total temporal duration of the shaper impulse response, the amplitude of this impulse response is proportional to the amplitude of the spectral response of the filter. If besides, the chirped FBG works within the Born approximation, the magnitude of the grating reflection spectral response $H_R(f)$ is approximately proportional to $\Delta n(z)$. Therefore, under these conditions, the shape of the grating apodization profile directly determines the temporal as well as the spectral shape of the output pulse. The desired temporal (or spectral) waveform only needs to be spatially "recorded" in the apodization mask used to write the grating. The application of this approach is limited to amplitude-only pulse shaping, and the time duration of the output pulses is limited by the length of the grating that can be written, typically in the nanosecond regime (corresponding to a physical fiber-grating length shorter than ~10 cm).

More advanced solutions for the use of FBGs as pulse shapers involve the use of general grating-synthesis algorithms, such as inverse-scattering or layer-peeling techniques [41–43], in order to determine the amplitude and phase profiles of the refractive-index modulation that are necessary to obtain a given temporal response. These methods allow one to design high-reflectivity FBGs to achieve the desired pulse-shaping operation, leading to increased energy efficiency.

Employing these gratings design techniques, FBGs have been designed to implement several optical signal-processing devices, which have been in turn employed, directly or indirectly, as optical pulse shapers:

Optical Differentiator An optical differentiator is a signal processing device that provide at its output the derivative of the complex envelope of an input optical signal. The ideal transfer function of an arbitrary order differentiator can be expressed as

$$H_{diff}(f) \propto j \cdot (f_{opt} - f_0)^N, \tag{9.10}$$

where $j = (-1)^{1/2}$ and N is the differentiator order. A number of different approaches for first- and high-order optical differentiators have been proposed based on FBGs operating in reflection, each of them trying to improve their operation bandwidth or spectral resolution within the practical limitations of the technology [49–52]. Optical differentiators have been employed for the generation of a first- and high-order Hermite-Gaussian (HG) optical pulses [53]. HG polynomials form a complete set of orthogonal temporal functions, a property that can readily be exploited in advanced coding for network access applications. Moreover, based on this property, a platform has been proposed for programmable arbitrary optical pulse shaping involving the addition of weighted first- and high-order derivatives of an input Gaussian-like pulse [32].

Optical Integrator Another important pulse processor whose implementation has been widely investigated based on FBG technology is the all-optical integrator. The optical integrator performs the cumulative time integral of the complex temporal envelope of an input arbitrary optical waveform. Its transfer function is

$$H_{int}(f) \propto \frac{1}{j \cdot (f_{opt} - f_0)^N}. \tag{9.11}$$

As with the case of the optical differentiator, a significant effort has been devoted to the development of broadband, high-resolution arbitrary order (N^{th}) optical integrators, and implementations based on passive and active configurations have been proposed and, in some cases, also experimentally demonstrated [54–59]. FBG-based optical integrators can readily be employed for the generation of unit-step time-domain functions and the implementation of flat-top pulse shapers, enabling reconfigurability of the flat-top temporal width [54, 57].

Optical Hilbert Transformer FBG-based Hilbert transformers (HT) have been also proposed and experimentally demonstrated [60–63]. A photonic HT is a pulse processor that provides the Hilbert transform of an incident optical pulse. The transfer function of an arbitrary order photonic HT is defined as

$$H_{HT}(f) \propto \begin{cases} e^{-jP\pi/2} & \text{if } f_{opt} > f_0, \\ 0 & \text{if } f_{opt} = f_0, \\ e^{jP\pi/2} & \text{if } f_{opt} < f_0, \end{cases} \tag{9.12}$$

where P is the fractional order. In the particular case of $P = 1$, the HT is integer. HTs, also known as phase shifters, are important components for a wide range of applications in the fields of computing and communications. As pulse shapers, HTs are particularly useful for generation of phase-shifted pulse doublets, where the order of the HT allows one to control the amplitude ratio between the two resulting pulse lobes.

Optical Coders/Encoders FBGs have been employed as time-domain coder/decoders for OCDMA systems [64–70]. Different approaches have been investigated, e.g., schemes based on arrays of uniform FBGs for generation of bipolar codes, requiring accurate controlled phase between individual gratings [64], or more compact schemes such as those based on superstructured FBGs [65–67] or step-chirped FBGs [68]. A reconfigurable scheme has also been proposed based on a simple uniform FBG with localized heating elements applied through thin resistive wires. These wires are able to apply different phase shifts by inducing impermanent chirp within a small confined segment of the FBG, eventually generating a desired phase code [69].

9.3.1.2 Fiber Bragg Gratings Operating in Transmission

Several implementations of optical pulse processors, and in particular optical pulse shapers, have been proposed recently using an FBG operating in transmission [71]. The use of FBG operating in transmission provides interesting advantages: transmissive FBGs avoid the requirement of an optical circulator or optical coupler to separate the output signal from the input, what reduces the complexity and cost of the processor unit. Also, they are more robust against fabrication errors due to the weak interaction

between the signal optical field and the grating when the signal is simply transmitted through the device (instead of reflected), so that imperfections in the grating are not directly "impressed" upon the signal field [87]. However, FBGs in transmission have an important drawback for their application as processing units based on the implementation of a prescribed complex spectral transfer function. The amplitude of the grating's linear spectral response in transmission $H_T(f)$ uniquely determines its phase by means of the Kramers-Kronig relationship, that is, the transmission spectral response is a minimum phase (MP) function [88]. Therefore, there is no freedom in choosing the complex spectral response to be implemented. In principle, only temporal shapes whose spectrum is an MP function can be implemented using this configuration.

Using the transmissive configuration, flat-top pulse shapers have been numerically proposed [72], as their required spectral response is an MP function

$$H_{ft}(f) \propto \text{sinc}\,(f \cdot \tau_{FWHM}), \tag{9.13}$$

where the sinc function is defined as $\sin(\pi f)/(\pi f)$, and τ_{FWHM} is the duration of the desired output flat-top pulse. Also, optical differentiators based on FBGs in transmission were proposed [73]. However, unpractical complex apodization profiles with high peak coupling strengths and a large number of precisely located discrete phase shifts are needed when the processing bandwidth exceeds ~100 GHz.

Alternatively, flat-top, parabolic and rectangular pulse shapers based on phase-modulated FBGs operating in transmission have been implemented [74]. This method relies on engineering the period profile $\Lambda(z)$ (instead of the apodization profile) to achieve the desired pulse shaping functionality in the transmissive spectral response of the FBG. This technique facilitates the grating fabrication process, as the coupling strength remains constant along most of the grating length. However, the fabrication constraints, such as the limitation in the spatial resolution, are transferred to the implementation of a user-defined relatively complex phase mask.

All the previously presented approaches for conventional FBG-based optical signal processing, and in particular optical pulse shaping, present a stringent operation bandwidth limitation. The processing bandwidth of FBGs is limited by the achievable spatial resolution of available fabrication technologies for tailoring the coupling coefficient profile along the grating length [36]. For instance, considering a typically feasible sub-millimeter resolution for the fiber grating apodization profiles, FBG-based pulse shaping implementations have been limited to temporal resolutions of at least several picoseconds, i.e., corresponding to a few hundreds of GHz in terms of frequency bandwidth of the generated output optical pulse shapes [36].

9.3.2 Long Period Gratings (LPGs)

Fiber LPGs are grating-assisted co-directional couplers, which induce coupling between the propagating core-mode and co-propagating cladding-modes of the optical fiber [35, 36]. These devices have recently attracted a great deal of interest for linear optical pulse shaping and processing applications. Thus similar building blocks as those ones introduced in the previous sections for FBGs, e.g., optical differentiators, integrators, Hilbert transformers and ultrafast pulse coders/decoders have been designed and implemented based on LPGs [75–79]. Those building blocks have been employed for a wide variety of signal-processing functionalities, including pulse-shaping applications. The

large bandwidth typical for these fiber filters allows scaling the filtering technique to the THz-bandwidth regime.

With regard to pulse processing work using LPGs, some interesting LPG-based optical code generation designs were first reported in [77] but they proved to be limited to the synthesis of temporally symmetric and binary intensity-only (on-off-keying, OOK) optical codes. Also, LPG-based differentiators have been reported and used for (sub-)picosecond optical pulse shaping [78, 79]. However, the pulse shaping based on this original approach is strictly limited to the generation of very specific waveform shapes, more prominently the generation of (sub-)picosecond flat-top and first- and high-order Hermite-Gaussian pulse waveforms from Gaussian-like optical pulses.

9.4 Recent Work on Fiber Gratings-Based Optical Pulse Shapers: Reaching the Sub-Picosecond Regime

Fiber gratings solutions offer interesting advantages that make them adequate technological components in recent and future communication systems. However, as reviewed in Section 9.3, they have also important drawbacks, such as the limited operation bandwidth and the lack of reconfigurability. In the last few years, a great deal of research has been carried out to find solutions that overcome those drawbacks, especially the limitation in the operation bandwidth. In this section, we describe the recent advances in the design and implementation of fiber grating-based pulse shapers that have enabled the achievement of ultrafast operation speed, i.e., well in the THz regime, corresponding to time resolutions down to the sub-picosecond regime.

9.4.1 Recent Findings on FBGs

FBGs have previously been used for many interesting optical time-domain linear signal-processing operations, such as optical pulse shapers, differentiators, integrators or Hilbert transformers. In general, FBG-based optical filters usually work in reflection. As introduced in Section 9.3.1, FBGs working in transmission directly overcome two of the constraints of reflective FBGs, i.e., avoiding the need for additional devices (e.g. circulators) and being more robust against fabrication errors. Recently, it has been demonstrated how transmissive FBGs are able to operate well in the THz regime without increasing the spatial resolution of the apodization profile, as detailed below. However, their main restriction is that the spectral transfer function is necessarily MP [88], imposing a very tight relationship (Hilbert transform) between the real and imaginary parts of the filter spectral response. Fortunately, an important, broad set of optical pulse processors (e.g. time differentiators, integrators) and shapers (e.g., for flat-top, triangular, parabolic pulse generation, among others) can still be realized using MP optical filters.

The design of a linear optical filter to be implemented in an FBG operating in transmission requires the specification of a prescribed minimum-phase spectral transfer function, $H_{ideal}(f)$. Thus, $H_T(f)$ must be proportional to $H_{ideal}(f)$ over the target operation bandwidth. In the notation used, $|H(f)|$ corresponds to the magnitude of the spectral response and $\arg(H(f))$ is the spectral phase.

In an MP filter (e.g., FBG in transmission), the filter's spectral phase response is necessarily determined by the desired spectral amplitude response by means of the

Kramers-Kronig relations. In addition, in an FBG, the transmissivity ($T = |H_T(f)|^2$) and reflectivity ($R = |H_R(f)|^2$) are necessarily related by $T = 1 - R$, due to the principle of conservation of energy. Thus, the specifications of $|H_T(f)|$ uniquely impose the functions $\arg(H_T(f))$ and $|H_R(f)|$. Therefore, from the specifications of the desired transmission amplitude spectral response, $|H_T(f)|$, the design problem reduces to synthesizing an FBG providing the reflection amplitude spectral response, $|H_R(f)|$, with no additional constraints on the FBG reflection spectral phase response, $\arg(H_R(f))$. Hence, the FBG reflection spectral phase can be suitably fixed to achieve the simplest grating design according to the target specifications. Among different possibilities, minimum-phase, maximum-phase, linear phase, quadratic phase, cubic phase profiles (and so on) can be used [71].

It has been demonstrated that the use of a reflective quadratic spectral phase enables the synthesis of arbitrary amplitude spectral responses over bandwidths well in the THz range using feasible and remarkably simple FBG apodization profiles [89]. Recall that a quadratic spectral phase corresponds to a linear group-delay profile. The desired linear group-delay in the FBG reflection response can be induced by introducing a quasi-linear grating-period variation (or grating-period chirp) along the device length. As the reflected frequency components along the grating are related to its period, the bandwidth of the spectral response in reflection, i.e. the corresponding rejected bandwidth in transmission, can then be significantly higher than in the uniform grating-period case.

Using this strategy, the FBG reflection spectral response to be synthesized can be mathematically expressed by

$$H_R(f) = W(f)\sqrt{R_{max}(1 - |H_T(f)|^2)} \cdot \exp\left\{j\left(\frac{1}{2}\ddot{\Phi}(2\pi f)^2 + (2\pi f)\tau_d\right)\right\}, \tag{9.14}$$

where R_{max} is the maximum peak reflectivity; $\ddot{\Phi}$ is the dispersion parameter (s^2) or equivalently, the slope of the group-delay curve as a function of the angular frequency; $W(f)$ represents a windowing function, which is introduced considering that the reflective response of an FBG must be a limited band-pass filtering function; and τ_d is a time delay introduced to make the device causal, generally equal to half the duration of the device impulse response, i.e. $\Delta t_1/2$. The dispersion parameter $\ddot{\Phi}$ will determine the minimum grating length L, according to the relationship:

$$\ddot{\Phi} = \frac{n_{eff}L}{\pi B c_0}, \tag{9.15}$$

being n_{eff}, the effective refractive index of the grating, and B the full-width reflection bandwidth of the device (Hz). From the target specifications defined by Eq. (9.14), the grating perturbation to be implemented, i.e., the apodization profile, can be obtained from a layer-peeling FBG synthesis algorithm, e.g., based on Coupled Mode theory combined with the Transfer Matrix method [41].

The dispersion parameter $\ddot{\Phi}$ is a fundamental design parameter which can be properly selected to ensure that the resulting grating apodization specifications match the fabrication constraints. In particular, a higher dispersion value translates into a more relaxed spatial resolution and a lower refractive index modulation peak, but requiring a longer device. It can easily be tuned by accordingly changing the slope of the linear grating-period variation (for a fixed operation bandwidth).

9.4.1.1 Minimum Phase Functionalities

The introduced approach has been exploited to design two relevant ultra-fast (THz-bandwidth) all-optical signal processing devices, in particular, first- and high-order differentiators [89,90] and a flat-top pulse shaper [89,91].

Optical Differentiators A first-order all-optical differentiator with a processing bandwidth of $B = 2$ THz (full-width at 0.1% of the maximum spectral amplitude) has been recently designed using the approach described above [89]. The dispersion parameter $\ddot{\Phi}$ was set to 80 ps^2, and R_{max} was set to 99.9999%. In this case, no windowing is required ($W(f) = 1$) as the reflective transfer function is inherently a band-pass function.

A synthesis tool [41] was employed to obtain the grating profile of the desired FBG-based optical differentiator from the specifications in Eq. (9.14), which is plotted in Figure 9.5 (a), in the color plate section. The synthesized grating device is readily

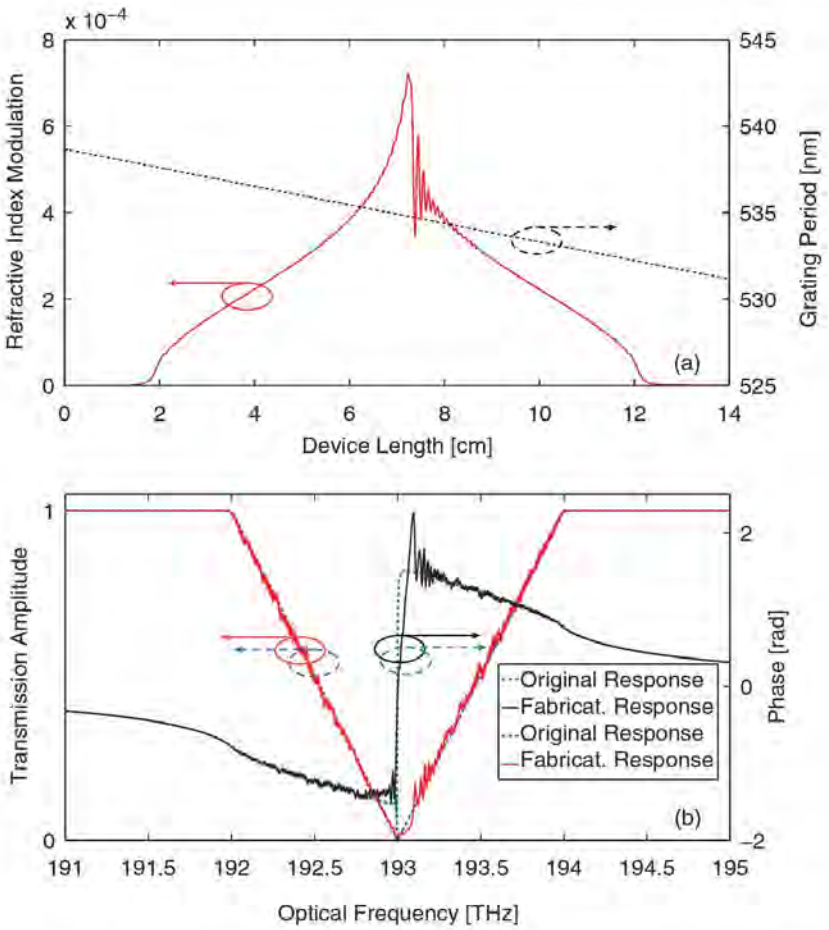

Figure 9.5 First-order optical differentiator based on an FBG in transmission: (a) Apodization (red solid line) and period (black dashed line) profiles considering realistic spatial resolution (limited to 0.3 mm) and linearly chirped phase mask; (b) Specified transmission spectral response, amplitude (dotted blue line) and phase (dotted green line) compared to fabrication-constrained transmission spectral response, amplitude (solid red line) and phase (solid black line). *Source*: María 2013 [89]. For a color version of this figure please see color plate section.

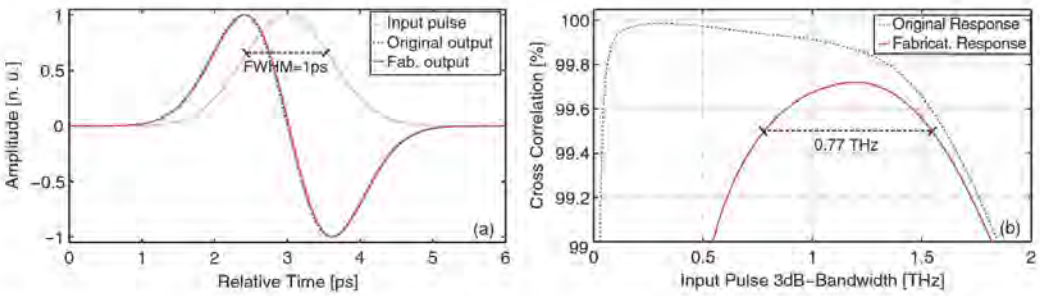

Figure 9.6 First-order optical differentiator based on an FBG in transmission: (a) Input Gaussian-like pulse (dotted black line) and comparison between the original output (dashed blue line) and the numerically obtained output from a differentiator adapted to fabrication constrains (red solid line); (b) Cross-correlation value between the ideal and the numerically obtained temporal output waveform as a function of the 3 dB-bandwidth of an input Gaussian pulse for the original design (blue dashed line) and the perturbed design considering fabrication limitations (red solid line). *Source*: María 2013 [89].

feasible with current fabrication technology, with (i) an effective length of 10.37 cm (as expected from Eq. (9.15)), (ii) a chirp value of −0.52 nm/cm, (iii) an amplitude-only apodization function with a peak refractive index modulation $\Delta n_{max} = 0.72 \times 10^{-3}$, and (iv) an average spatial resolution of the ripples in the apodization profile of ~ 0.3 mm. Therefore, the fabrication parameters were significantly relaxed as compared with previous designs based on uniform-period transmission gratings [73], while the achievable processing speed was increased in one order of magnitude. The robustness of the design was analyzed by evaluating the sensitivity of the grating transmission spectrum to realistic fabrication constraints, i.e., sub-millimeter resolution of the apodization profile and maximum refractive index modulation $< 10^{-3}$, shown in Figure 9.5 (b) in the color plate section.

Figure 9.6 (a) presents the comparison between the original expected output signal and the output from an FBG with typical fabrication constrains, showing an excellent match between the two curves. Besides, as observed in Figure 9.6 (b), the differentiator performance, estimated by its TBP, is mainly degraded for wider temporal input pulses (corresponding to frequency bandwidths narrower than 0.5 THz) while preserving a coefficient higher than 99.5% when the input pulse has a 3 dB-bandwidth ranging between 0.78 and 1.55 THz (TBP $\sim$ 2). This fact is predominantly attributed to the deviations between the original and fabrication-constrained device spectral responses around the transmission resonance notch.

The design of 2 THz higher order (up to $N = 4$) optical differentiators was also proposed based on the same design methodology, shown in Figure 9.7 [90]. All the design parameters were set to similar values to those ones from the previous example. Only the specified transmission deep varies from −60 dB from the first order to −90 dB for the fourth order. Numerical simulations are used to evaluate the output temporal waveforms when a Gaussian-like 850 fs-FWHM input pulse is launched at the input of the FBG. Figure 9.7 (b) shows the first-to-fourth order derivatives of the input pulse, exhibiting an excellent agreement with the expected output waveforms of the ideal differentiators.

Optical Pulse Shapers Picosecond flat-top (rectangular-like) optical pulse shapers, over full-width spectra in the THz regime, have been designed and implemented using

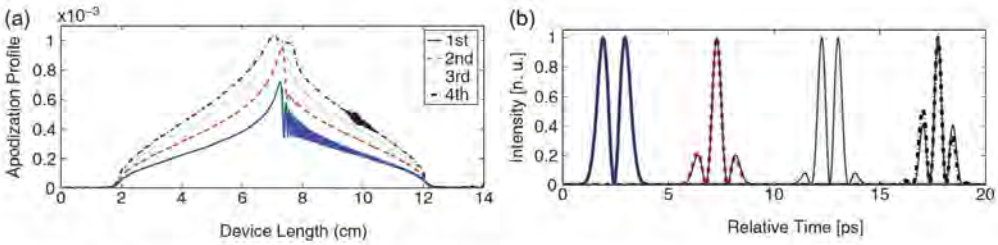

Figure 9.7 N^{th}-order optical differentiators based on FBGs in transmission: (a) Apodization profiles considering realistic spatial resolution (limited to 0.5 mm); (b) Intensity outputs from practical FBG-based differentiators. *Source*: María 2012 [90]. Reproduced with permission from IEEE.

transmission FBGs [89,91]. Assuming a sufficiently short Gaussian input pulse, the output will be a flat-top pulse if the filter provides an spectral transfer function approaching the ideal sinc function (Eq. (9.13)).

For the fabrication of the linearly-chirped-FBG, a 14.5 cm-long phase mask was used, with a period of 1064.05 nm (i.e., grating Bragg wavelength of 1544.87 nm) and a chirp of 2.5 nm/cm. These parameters fixed the dispersion-induced in the grating to $\ddot{\Phi} = 33.77$ ps^2. The target output temporal waveform was set to be a 2-ps flat-top optical pulse, and therefore, $\tau_{FWHM} = 2$ ps. In this case, a raised cosine function was employed as a window function $W(f)$. The full-bandwidth of $W(f)$ (measured at 0.1% of the maximum reflectivity) was chosen to be 5 THz. The output pulse spectrum was then fixed to extend over a full width of ~5 THz, thus including a few sidelobes of the sinc function. R_{max} was set to 99.99% (transmission dip of −40 dB).

Applying the synthesis tool to this prescribed reflection spectral response, the apodization and period profiles shown in blue in Figures 9.8 (a) and (b) in the color plate section were obtained. The synthesized device has an effective length of 11 cm with a peak refractive index of $\Delta n_{max} = 1.2 \times 10^{-3}$. Due to the expected limitation in the fabrication resolution, the apodization profile has been smoothed to have a conservative spatial resolution of 1 mm. The smoothed grating-apodization profile used

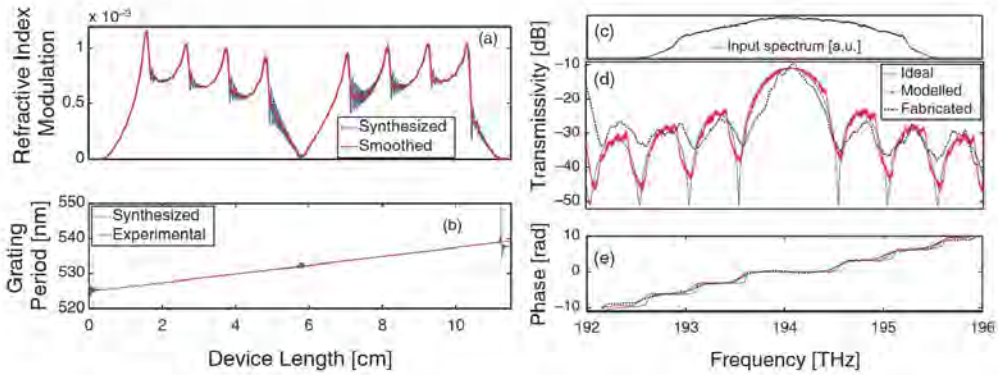

Figure 9.8 Flat-top pulse shaper based on an FBG in transmission: Obtained apodization profile (a) and period (b) from synthesis (blue line) and smooth profiles adapted to fabrication constrains (red line); (c) Input signal spectrum; (d) tranmissivity and (e) transmission phase response: ideal (blue line), simulated considering fabrication constraints (red line) and measured from fabricated device (dotted black line). *Source*: María 2013 [91]. For a color version of this figure please see color plate section.

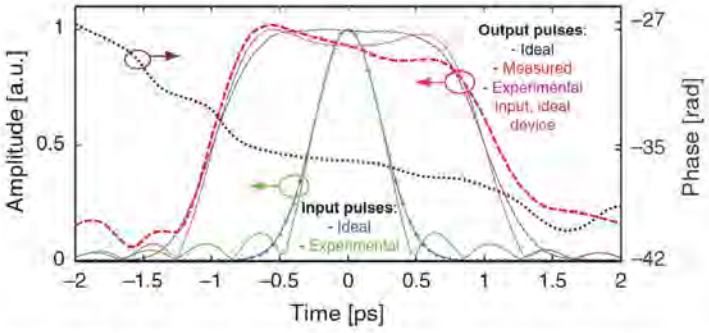

Figure 9.9 Flat-top pulse shaper based on an FBG in transmission: Temporal input response: ideal (blue line) and employed in the experiment (green line); Temporal output: ideal (black dashed-dotted line) and experimentally measured (red dashed line). *Source*: María 2013 [91]. For a color version of this figure please see color plate section.

for the linearly-chirped-FBG fabrication, as well as the linear period profile provided by the employed phase mask, are shown in red in Figures 9.8 (a) and (b). Notice that no additional phase variations are needed on top of the linear grating period chirp.

Based on the calculated refractive index profiles, the linearly-chirped-FBG were fabricated via UV illumination of hydrogen-loaded specialty single-mode fiber (UVS-INT from Coractive) by a frequency-doubled argon-ion laser operating at 244 nm through the described linearly-chirped phase mask. The designed refractive index apodization was implemented by dithering the phase mask during the fiber scan in order to control the visibility of the interference pattern while keeping the average refractive index constant. Figures 9.8 (d) and (e) show the resulting transmissivity and transmission phase compared with the specified ideal ones.

For full time-domain characterization, a Fourier transform spectral interferometry (FTSI) [92] scheme was implemented. The input and output temporal waveforms are plotted in Figure 9.9 in the color plate section. The device is optimized for an input Gaussian-like pulse with a FWHM of 400 fs, depicted in blue in Figure 9.9. A comparison between the measured data (red line) and the target data (black line) shows a good agreement between the ideal and the experimentally obtained pulse, confirming the capability of the fabricated grating for the target ultrafast pulse-shaping application. The FWHM of the measured output pulse's amplitude is 2.1 ps. The 5-THz operation bandwidth provides a rising/decaying time (measured between the 10% and the 90% of the maximum amplitude) of ~0.5 ps.

9.4.1.2 Non-Minimum Phase Functionalities (Arbitrary Optical Pulse Processors)

In spite of the important advantages of using FBGs operating in transmission, they still have a fundamental limitation, which is the fact that their linear spectral response is necessarily MP. An important body of research has been carried out to explore the possibility of implementing non-MP functionalities based on transmissive BGs [71, 93]. However, the extremely restrictive MP condition has severely limited the functionalities susceptible to be implemented using this configuration.

Recently, a general approach that enables the implementation of an arbitrary linear optical pulse processing functionality, generally requiring a non-MP filtering response (in which the amplitude and phase spectral profiles need to be tailored independently)

has been presented using a MP optical filter [94]. This approach is based on the fact that any causal temporal function with a dominant peak around or close to the origin will be either an MP function or close to one [39,95,96]. Based on this general property, the proposed design procedure involves creating a temporal impulse response that satisfies the MP condition by simply introducing an instantaneous component, e.g., a Dirac delta function $\delta(t)$, before the target non-MP impulse response [95,96]. The resulting impulse response is

$$h_{MP}(t) = K_1\delta(t) + K_2 h_{NMP}(t - \tau_G), \tag{9.16}$$

where τ_G is the time delay between the instantaneous component and the target non-MP impulse response, and $K_i, i = 1, 2$ are the weights given to each of the components of $h_{MP}(t)$, which determine the signal energy distribution at the system output. The spectral transfer function corresponding to this impulse response is MP and given by

$$H_{MP}(f) = K_1 + K_2 H_{NMP}(f)\exp\{-j2\pi f\tau_G\}. \tag{9.17}$$

Notice that the resulting spectrum from Eq. (9.17) looks like an interferometric pattern where the spectral phase information is coded in the phase variations of the resulting cosine-like spectral profile. A formal proof on the MP property of the transfer function defined by $H_{MP}(f)$ can be found in [96].

$H_{MP}(f)$ can be then synthesized by means of an FBG operating in transmission. Hence, $H_T(f)$ must approach $H_{MP}(f)$ over the device's operation bandwidth. To completely define $H_T(f)$, the constants K_1 and K_2 have to be calculated considering the grating physical constraints. On the one hand, since an FBG is a passive device, the maximum transmissivity $T_{max} = 1$, and consequently

$$|H_T(f)| \leqslant \sqrt{T_{max}} \rightarrow K_1 + K_2 \leqslant 1. \tag{9.18}$$

On the other hand, the maximum reflectivity R_{max} achieved by the device imposes a limitation on the minimum of $|H_T(f)|$

$$|H_T(f)| \geqslant \sqrt{1 - R_{max}} \rightarrow K_1 - K_2 \leqslant \sqrt{1 - R_{max}}. \tag{9.19}$$

This inequality becomes strict if $R_{max} = 1$ to avoid singular points in $H_{MP}(f)$. As a 100% reflectivity peak cannot be usually achieved in practice, K_1 and K_2 are obtained by solving the equation system defined by Eqs. (9.18) and (9.19) with the equality signs, thus optimizing the amount of energy that is transferred into the non-MP portion of the output signal. Nearly 50% of the output signal energy could be transferred into the non-MP portion as the maximum reflectivity approaches 100%.

This manipulation of the system response can generally be carried out as long as the target functionality can be restricted over a well-defined, finite time window, e.g., such as arbitrary short pulse processing and re-shaping operations. The signal at the output of the FBG is composed of two terms, one is a scaled version of the input signal, and the second one is proportional to the output of the non-MP processor, i.e., the desired processed waveform. In order to be able to recover the desired processed waveform, these two components must be properly separated in time. Therefore, the time delay τ_G between the delta function and $h_{NMP}(t)$ in Eq. (9.16) must be suitably designed, which essentially imposes a limitation on the input and output signal temporal durations. This design restriction will translate into a constraint in the maximum processing temporal

window of the device. The processing time window is directly related to the separation between the two components of the MP impulse response, which is only limited by the spatial resolution of the apodization profile. Depending on the target application, the desired processed waveform may need to be extracted through an additional temporal modulation process.

Optical Hilbert Transformer To demonstrate the potential of the proposed method for encoding an arbitrary phase shift in the device response, the realization of two HTs, an integer, i.e., $P = 1$ and a fractional one, $P = 0.81$ (see Eq. (9.12)) has been experimentally demonstrated [97]. In both cases, a phase mask with a grating chirp of 1.25 nm/cm and a length of 7 cm was employed for fabrication. $W(f)$ was chosen to be a raised cosine function with a full-width bandwidth (measured at 1% of the maximum amplitude) of 3.4 THz. However, different maximum reflectivities R_{max} were imposed for the two devices, in order to evaluate the influence of grating strength or peak reflectivity in the HT device performance, as discussed below. Thus, the integer HT has $K_1 = 0.88$ and $K_2 = 0.11$, corresponding to a peak reflectivity $R_{max} = 0.4$. The fractional HT has $K_1 = 0.97$ and $K_2 = 0.02$, corresponding with $R_{max} = 0.12$. The reflectivity and group delay in reflection of the integer HT are plotted in Figures 9.10 (a) and (b), dashed black curves. The power spectral response follows the anticipated interferogram-like profile with a nearly uniform envelope, corresponding to the constant amplitude spectral response of the all-pass HT filter; the phase shift in the middle of the sinusoidal interferogram profile corresponds to the target discrete shift in the phase spectral response of the HT filter. To facilitate the practical implementation of the resulting profile, the desired spectral response was practically achieved using two superimposed, unapodized, linearly chirped FBGs in a Fabry-Perot configuration [98], i.e., where the gratings are suitably spatially shifted with respect to each other. In particular, the induced Δn_{max} was $\backsim 2.5 \times 10^{-4}$ and the induced shift between gratings was $\backsim 1.7$ mm. This value of shift impose $\tau_G \backsim 17$ ps. Besides, one of the gratings that compose the Fabry-Perot structure must have a phase transition of π rad (integer case) and 0.81π rad (fractional case) at the

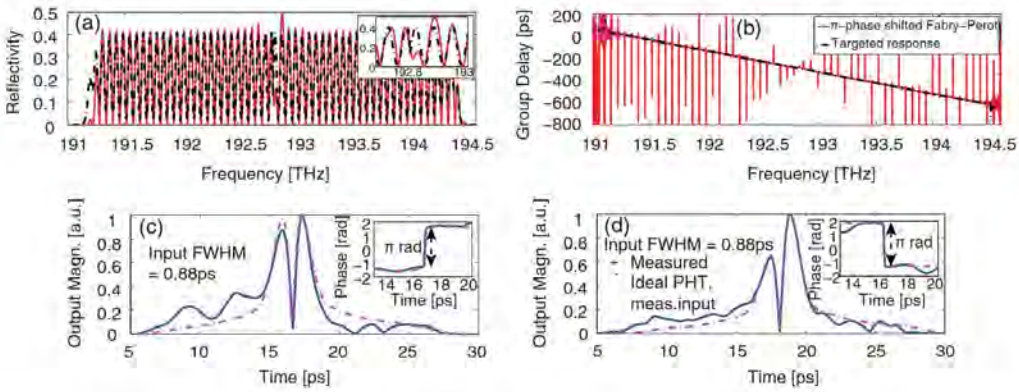

Figure 9.10 (a) Reflectivity and (b) group delay of a HT implemented in an FBG in transmission. The dashed black line represents the specified spectral response and the red line represents the spectral response of an FBG-based π-phase shifted Fabry-Perot structure. Measured output component of the fabricated integer (c) and fractional (d) HTs (solid line) for an input Gaussian-like pulse with a FWHM of 0.88 ps, as compared with the ideally expected output (dashed line). *Source*: María 2015 [97].

center of its length. The comparison between the target spectrum for the integer photonic HT and the reflective spectral response of the FBG-based Fabry-Perot structure is plotted in Figures 9.10 (a) and (b).

The gratings were fabricated following the same procedure as in the previously presented flat-top pulse shaper. In this case, the UV beam first swept a linearly-chirped phase mask with the required phase shift at the middle of its length. Then, a second linearly-chirped phase mask without phase shift was scanned by the UV beam with the same average power and sweep time to achieve the same refractive index modulation as the first grating.

The full time-domain characterization of the fabricated devices was realized by means of an FTSI scheme [92]. The employed input optical source consists of an optical parametric oscillator (OPO) followed by a tunable Gaussian-like band-pass filter. Figures 9.10 (c) and (d) (solid curves) provide the temporal output profiles measured by the FTSI method for input pulse width of 0.88 ps at FWHM for the cases (c) integer HT and (d) 0.81-order HT. The dotted-dashed lines in Figure 9.10 (c) and (d) are for the numerically simulated ideal outputs from the HTs. There is a good agreement between the obtained temporal waveforms and the output of the ideal HTs. The observed leading-edge tails in the integer HT is attributed to the non-uniform, irregular envelope of the interferogram-like pattern of the device transmissive spectral response. On the other hand, the 0.81-order fractional HT offers an improved performance, as observed in its time-domain characterization result, where the leading-edge trails are much less pronounced than for the integer HT. This fact is attributed to the lower reflectivity imposed for this grating.

In this case, the TBP is ~15, which is in line with previously presented photonic HTs based on FBG in reflection [60–63], but providing an operation bandwidth one order of magnitude higher.

9.4.2 Recent Findings on LPGs

The focus of this section is on a recently developed THz-bandwidth *arbitrary* optical pulse shaping theory and technique using fiber LPG devices [99–101]. This solution enables one to synthesize/process optical waveforms with temporal resolutions well into femtosecond range, i.e., faster operation speeds (bandwidths) than conventional FBG-based optical waveform generation and processing schemes. The most striking feature of the introduced novel theory, referred to as *superluminal space-to-time mapping* in LPGs, is that the achievable temporal resolution of the proposed LPG-based optical waveform generation and processing scheme is not limited by the spatial resolution of the grating fabrication technologies.

In all fiber grating devices, the processing or synthesis of faster temporal features necessarily requires the use of smaller spatial resolutions in the grating complex apodization profile [35,36]. This space-time relationship is more evident in FBGs working in reflection under weak-coupling condition (first-order Born approximation). As discussed in Section 9.3, in this case the output time-domain filter response $h(t)$ (complex envelope) is directly proportional to the complex grating apodization profile $\Delta n(z)$ with a space-to-time scaling factor directly determined by the classical light propagation laws through the medium. However, as expected for any light propagation-based process, in this scheme, the ratio (v) between the space (Δz) and time (Δt) variables is necessarily

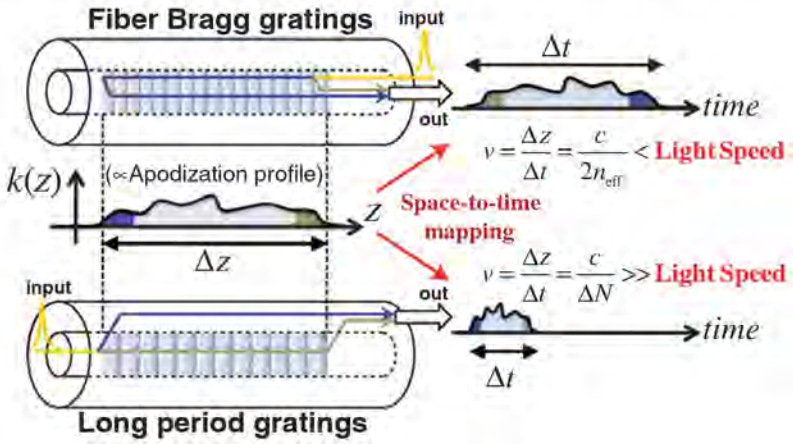

Figure 9.11 Illustration of the space-to-time mapping phenomena in FBG and LPG cases, respectively. *Source*: Ashrafi 2013 [99].

lower than the propagation speed of light in vacuum (c_0) [37], i.e. $v = \Delta z/\Delta t < c_0$, in particular $v = c_0/2n_{eff}$, where n_{eff} is the average effective refractive index of the propagating mode in the FBG (see Figure 9.11). As a result, the achievable temporal resolution must be necessarily larger than the light-wave propagation time through the minimum spatial feature of the grating apodization profile, as determined by the spatial resolution of the used technology. That leads to FBG devices for optical signal processing/synthesis being limited to temporal resolutions of at least several picoseconds, considering a typically feasible sub-millimeter resolution for the fiber grating apodization profiles.

It has recently been found [99] that a similar space-to-time mapping phenomenon can be observed under weak-coupling condition (Born approximation) in the case of LPGs, see illustrations in Figure 9.11. In contrast to FBG devices, it has been demonstrated that the space-to-time mapping speed ($v = \Delta z/\Delta t$) in a LPG device can be significantly higher than the speed of light in vacuum. This new finding is referred to as superluminal space-to-time mapping [99]. An obvious consequence of this phenomenon is that LPGs can be designed for processing/synthesis of optical waveforms with temporal features orders of magnitude faster (shorter) than those achievable using counter-directional coupling devices assuming the same practical spatial resolution limitations in grating fabrication.

For the analysis of the space-to-time mapping approach in LPGs, it is assumed that the LPG-induced coupling occurs predominantly between the fiber core mode and a single cladding mode. A comprehensive analysis of this approach can be found in [99]. The basis of the concept is briefly revisited in what follows. Under the weak-coupling condition, the cross-coupling spectral transfer function $H_{c-cl}(f)$ at the output end of the LPG (i.e., at Δz) is

$$H_{c-cl}(f) \backsimeq j \int_0^{\Delta z} |k(z)| e^{-j(2\pi f)z\Delta N/c_0} dz. \tag{9.20}$$

In Eq. (9.20), $k(z)$ is the complex coupling coefficient defined as $k(z) = |k(z)| \exp\{j\Phi(z)\}$, where $|k(z)| = (\Delta n(z)\pi f_0)/c_0$ accounts for variations in the coupling strength along the waveguide axial (light propagation) direction (z) and $\Phi(z) = 2\pi \int (1/\Lambda(z) - 1/\Lambda_0)dz$ accounts for local grating period variations along z.

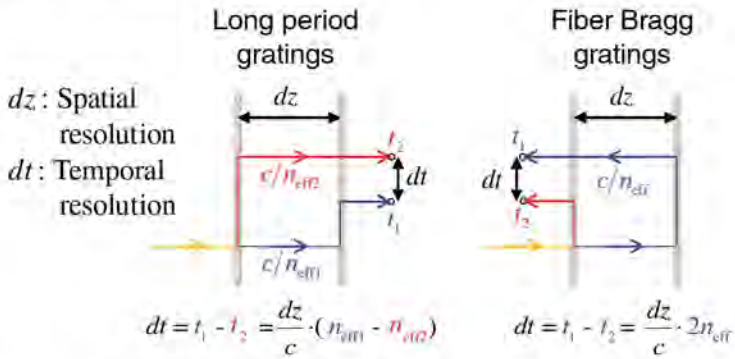

Figure 9.12 Illustration of the temporal resolutions (*dt*) that are associated with a prescribed spatial resolution (*dz*) in the grating apodization profile for the FBG and LPG cases. In each case, the temporal resolution is defined by the difference between the arrival times of the impulses coupled at the input and output ends of the corresponding spatial-resolution element. *Source*: Ashrafi 2013 [99].

Also, $\Delta N = n_{eff1} - n_{eff2}$, where n_{eff1} and n_{eff2} are the average effective refracting indices of the two interacting modes. On the other hand, based on the Fourier transform theory, $H_{c-cl}(f)$ can be also expressed as

$$H_{c-cl}(f) = \int_0^{\Delta t_1} h_{c-cl}(t) e^{-j(2\pi f)t} dt, \tag{9.21}$$

where Δt_1 is the full time-width of the cross-coupling impulse response. By comparing Eqs. (9.20) and (9.21), it can be inferred that

$$h_{c-cl}(t) \propto \left\{ |k(z)| e^{j\Phi(z)} \right\}_{z=tc_0/\Delta N}. \tag{9.22}$$

Therefore under weak-coupling condition, the cross-coupling temporal impulse response of the fiber LPG is approximately proportional to the variation of the complex coupling coefficient $k(z)$ as a function of the grating propagation distance z after a suitable space-to-time scaling. In particular, the space-to-time mapping speed (v), is obtained as $v = c_0/\Delta N$. Clearly, ΔN can be made much smaller than 1 and consequently, the resulting speed can be made significantly higher than the speed of light in vacuum.

Figure 9.12 illustrates the physical principle of the obtained space-to-time mapping law in FBGs as compared with the case of LPGs. The described phenomenon enables a direct mapping of the grating apodization profile along the device's temporal impulse response. This leads to straightforward, simple grating designs providing the desired linear temporal response. This design strategy should be particularly useful for devices aimed at re-shaping an ultra-short optical pulse (temporal impulse launched at the device input). Most importantly, on the basis of the superluminal space-to-time scaling law, ultrashort temporal features can be achieved using greatly relaxed spatial resolutions, i.e., time features much faster than those intrinsically imposed by the fundamental light propagation laws through the medium, by properly designing the effective refractive index difference between the two interacting modes.

An important practical consideration concerns the fact that the input and output signals must be carried by two different waveguide modes. In an integrated-waveguide approach [102], the device could be practically implemented by using two physically

separated single-mode optical waveguides. All-fiber LPGs are typically based on coupling between the core mode (easily extracted from the fiber) and a cladding mode. Traditionally, in order to transfer the cross-coupling signal in the fiber cladding-mode to the fiber core-mode, it was necessary to concatenate a core-mode blocker and a short, strong uniform LPG [75]. In a recent experimental implementation of the LPG-based pulse shaping approach, a novel alternative technique to extract the cross-coupling signal from the LPGs by splicing a suitably misaligned fiber has been employed [101].

9.4.2.1 Triangular and Parabolic Pulse Shapers

The LPG to perform the optical pulse shaping must properly apodized along its length and operates in the cross-coupling mode (e.g., single-mode fiber LPG working in the core-to-cladding operation mode). The complex apodization profile, i.e., $\Delta n(z)$, must be a spatial-domain scaled version of the target output temporal pulse waveform, i.e. $h_{c-cl}(t)$, with a space-to-time scaling law defined by Eq. (9.22). The capability of the introduced optical pulse shaping approach for the generation of two ultra-fast optical arbitrary waveforms has been demonstrated in [99], namely saw-tooth and parabolic pulses, down to the femtosecond regime using feasible LPG designs, i.e., with mm resolutions.

Standard single-mode fiber (Corning SMF-28) has been considered the optical waveguide platform. Also the same LPG design parameters as the well experimentally characterized LPG made on SMF-28 in [103] have been considered. The grating period is $\Lambda = 430\,\mu m$, which corresponds to coupling of the fiber core mode into the LP06 cladding mode at a central wavelength of 1550 nm [103]. The following wavelength dependence has been assumed for the effective refractive indices of the two coupled modes [103]: $n_{0,1}(\lambda) = 1.4884 - 0.031547\lambda + 0.012023\lambda^2$ for the core mode and $n_{0,6}(\lambda) = 1.4806 - 0.025396\lambda + 0.009802\lambda^2$ for the cladding mode, where $1.2 < \lambda < 1.7$ is the wavelength variable in μm. The spectral responses of the LPG designs are numerically simulated using the Coupled Mode theory combined with a Transfer Matrix method [35].

The LPG apodization profiles along the grating structure for implementation of the sub-picosecond optical triangular and parabolic waveform generations are shown in Figure 9.13 (a) and (b) respectively. Three LPGs with the same length and different maximum refractive index modulation have been simulated for each pulse shaper (LPG 1-3 for triangular and LPG 4-6 for parabolic pulse shapers). The corresponding simulation results for power spectral responses of the designed LPGs are presented in Figure 9.13 (c) and (d) respectively. The corresponding temporal responses of the designed LPGs to an ultrashort input Gaussian pulse with 100 fs full-width at 10% of the peak amplitude, are shown in Figures 9.13 (e) and (f) respectively. The simulation results reveal that the designed LPGs implement very nearly the desired pulse re-shaping operations even when the weak-coupling strength condition is clearly not satisfied, see the results corresponding to the design cases with the highest maximum coupling coefficient in Figure 9.13, making a nearly 100% cross-coupling peak.

9.4.2.2 Tsymbol/s Phase Coding

Optical pulse encoding and decoding techniques have been extensively investigated for a wide range of optical processing applications. These techniques are particularly interesting for applications requiring the generation of time-limited data streams (composed

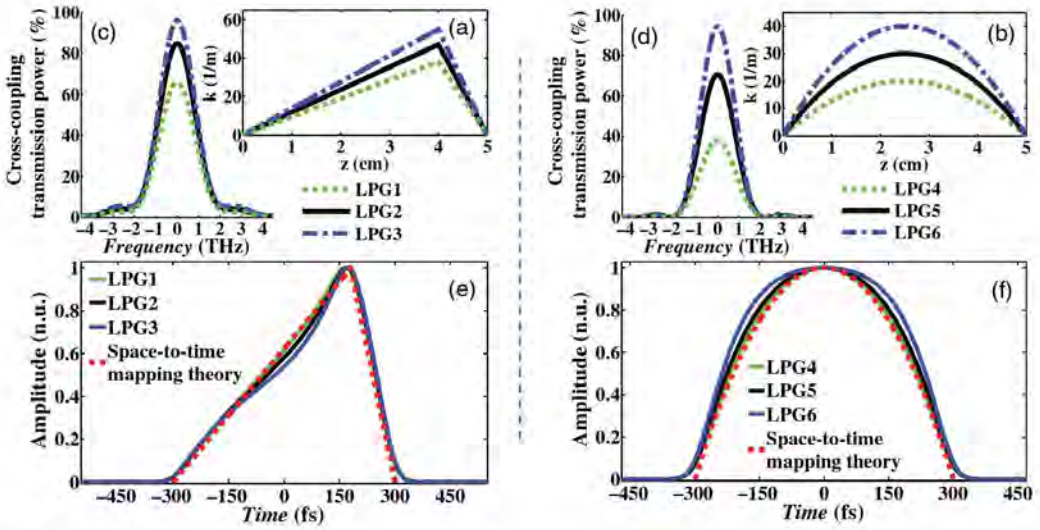

Figure 9.13 (a,b) The apodized-LPG designs for femtosecond optical saw-tooth and parabolic waveform generation respectively. (c,d) The corresponding simulation results for spectral power responses of the designed LPGs. (e,f) The corresponding simulation results for temporal responses (complex envelopes) of the designed LPGs to an ultrashort (~100fs) Gaussian pulse. *Source*: Ashrafi 2013 [99].

of a few consecutive symbols), such as OCDMA and optical label-switching communications [68,70].

The capability of the superluminal space-to-time mapping approach for generation of customized serial optical communication streams under any desired complex coding format well in the Tsymbol/s range (femtosecond resolutions) was shown in [99], where readily feasible LPG designs, e.g., with grating apodization resolutions above the millimeter range were used.

Figure 9.14 shows the numerical simulation of an LPG design for generation of 8-symbol optical QPSK signals with a speed of 4 Tsymbol/s (4 TBaud), from an input ultra-short optical Gaussian pulse with a (full-width at 10% of the peak amplitude) duration of 100 fs. The simulation method and the LPG design parameters is the one used in

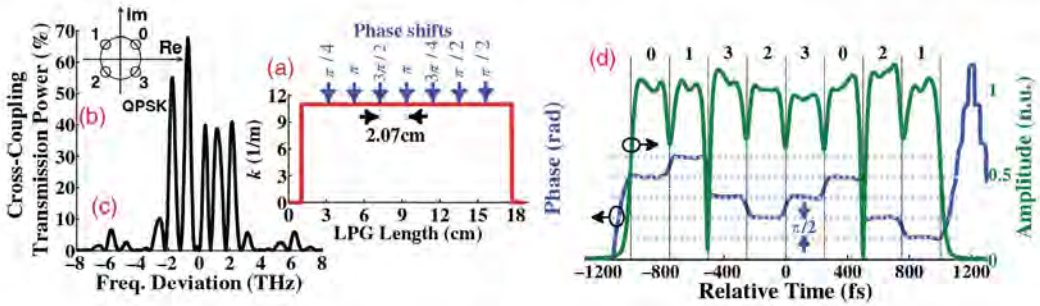

Figure 9.14 Simulation results of the designed LPG (a) to generate 8-symbol optical QPSK (b) data stream patterns, i.e. ''0''1''3''2''3''0''2''1'', with a speed of 4 Tsymbol/s from an input (full width at 10% of the peak amplitude) 100 fs optical Gaussian pulse. (c) The corresponding spectral power responses of the designed LPGs. (d) The corresponding output temporal amplitude and phase responses. *Source*: Ashrafi 2013. Reproduced with permission of Scientific Research.

previous section. In particular, Figure 9.14 (a) shows the designed amplitude and phase grating-apodization profiles for the target QPSK coding operation. The grating design is relatively straightforward and simple, just being spatial-domain mapped versions of the respective targeted complex time-domain optical data stream. Figure 9.14 (d) shows the amplitude and phase profile of the time-domain waveforms at the output of the simulated LPG design, demonstrating accurate generation of the targeted 4 Tsymbol/s data streams, as per the coding formats defined in Figure 9.14 (b), in excellent agreement with the inscribed grating-apodization profile (Figure 9.14 (a)).

The spectral power response of the designed LPG filter is shown in Figure 9.14 (c). It is worth mentioning that the complexity of this spectral response (also for the phase, not shown here) increases for a larger number of symbols (and for a higher number of amplitude and phase levels in each symbol), making it very challenging for practical implementation using a frequency-domain filter synthesis approach, e.g. conventional programmable linear wave-shapers with limited spectral bandwidth and resolution. In contrast, the proposed superluminal space-to-time mapping approach bypasses the mentioned spectral complexity by directly mapping the simpler filter time-domain impulse response along the grating spatial profile.

Following the previous design methodology, several data pulse sequences have been experimentally demonstrated. As shown in Figure 9.11, the input and output signals must be carried by two different waveguide modes, namely the core-mode and a cladding-mode in a typical fiber-optics configuration. The LPGs are designed for generation of different 4-bits pulse data streams, i.e. ''1''0''0''1, ''1''0''0''−1'' and ''1''0''1''1'', respectively, with a target speed of ~3.5 Tbit/s. In each case, the target temporal pattern is directly mapped along the grating complex coupling-coefficient (apodization) profile of the corresponding LPG, see Figures 9.15 (a)–(c) in the color plate section. The three LPGs revisited here were fabricated via UV illumination of hydrogen-loaded single-mode fiber (Corning SMF28) by a frequency-doubled argon-ion laser operating at 244 nm through an amplitude mask [104].

The reported patterns are specifically designed to demonstrate the anticipated space-to-time mapping process for both amplitude and phase profiles. Whereas the patterns ''1''0''0''1 and ''1''0''1''1'' exhibit a different amplitude variation, the target is that all the pulses in these streams are in phase, requiring in-phase LPGs. Additionally, a pattern ''1''0''0''−1'', where the two pulses at the extremes of the pulse code sequence need to be exactly out of phase, was targeted. The required π-phase-shift has been implemented by use of an amplitude mask having a half-period shift in the middle of its length. In all the reported designs, the grating period is 430 μm which corresponds to coupling of the fundamental core-mode into the LP06 cladding-mode at a central wavelength of 1550 nm [103].

The average effective refractive indices of the fundamental core-mode and LP06 cladding-mode in the SMF-28 fiber around 1550 nm are $n_{eff1} = 1.4684$ and $n_{eff2} = 1.4648$, respectively [103]. The predicted space-to-time mapping speed in the fabricated LPGs is then $v = c_0/\Delta N = 833 \times 10^8$ m/s, which is about ~278 times larger than the speed of light in vacuum. The separation length between the first and last apodization-bits of the fabricated LPGs is ~7.12 cm, see Figure 9.16 (a)–(c), and the total length of the LPG devices is ~9.5 cm, which corresponds to the target bit-rate of 3.5 Tbit/s. According to numerical simulations, LPGs exhibit refractive index modulation amplitudes (half of the peak-to-peak value) of 9.9×10^{-5}, 1.1×10^{-4} and 6.7×10^{-5} for the cases shown in

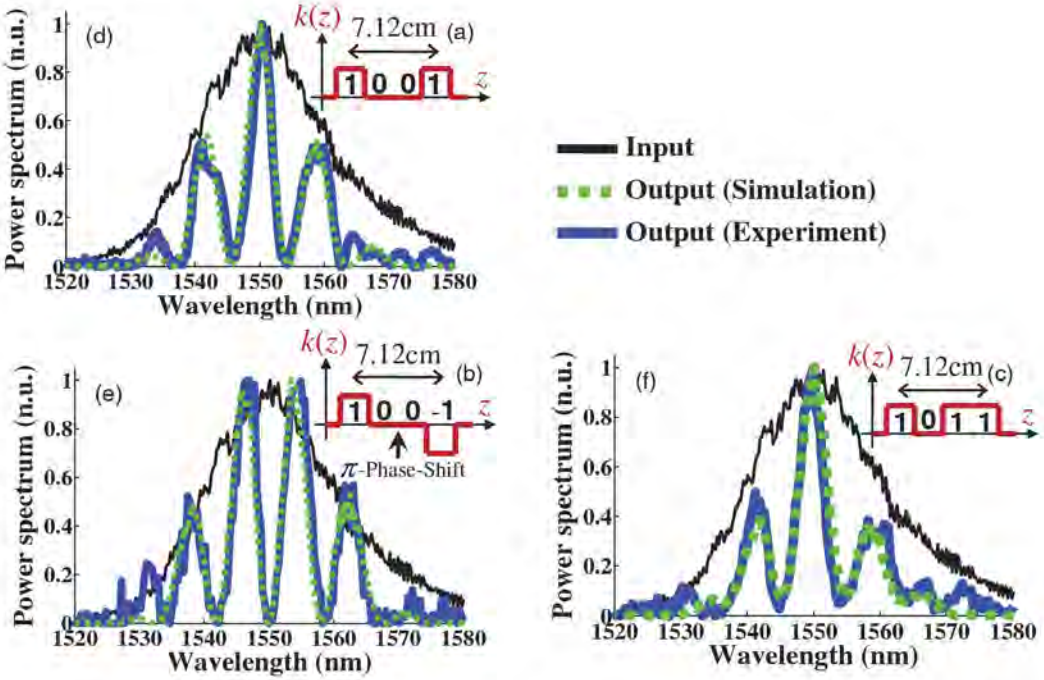

Figure 9.15 (a–c) Fabricated fiber LPG designs for generation of 4-bit data streams, i.e. ''1''0''0''1, ''1''0''0''–1'' and ''1''0''1''1'', respectively, with a target speed of ~3.5-Tbit/s. (d–f) The corresponding experimental spectrum measurements of the femtosecond optical pulse from the OPO laser before (solid black curves) and after (solid blue curves) propagation through the fabricated LPGs, compared with the simulated linear spectral responses of the LPGs (dotted green curves) to the same input OPO laser pulse spectrum. The spectra are represented in normalized units (n.u.). *Source*: Ashrafi 2013 [101]. For a color version of this figure please see color plate section.

Figures 9.15 (a)–(c), respectively. The peak transmission power of the core-to-cladding spectral responses of the fabricated LPGs is as high as 80% (i.e., corresponding to measured resonance depths of ~7 dB in core-to-core transmissions). Whereas the space-to-time mapping theory is strictly valid under weak-coupling strength condition [99], this is clearly not satisfied in these designs. Simulations have revealed that for the target outputs, LPGs with a strong coupling strength can still implement very nearly the desired pulse shaping operations while improving the devices' energy efficiency.

The experimental setup for time-domain characterization of the fabricated LPGs is based on FTSI, which is used to retrieve the phase and amplitude profiles of the complex temporal waveforms at the LPGs' outputs [105], using the input optical pulse itself as the reference in the measurement setup. The input optical pulse is a nearly transform-limited Gaussian-like optical pulse directly generated from an OPO, which is also used as the reference signal in the interferometric setup. The input pulse from the OPO laser is estimated to have a FWHM time-width of ~200 fs (and a FWHM spectral bandwidth of ~22 nm). The carrier wavelength of the optical pulse is tuned at the resonance wavelength of the LPGs, i.e. 1550 nm. The normalized measured spectra of the optical pulse before and after the fabricated LPGs are shown in Figure 9.15 (d)–(f). The experimentally recovered time-domain amplitude and phase profiles at the output of the LPGs

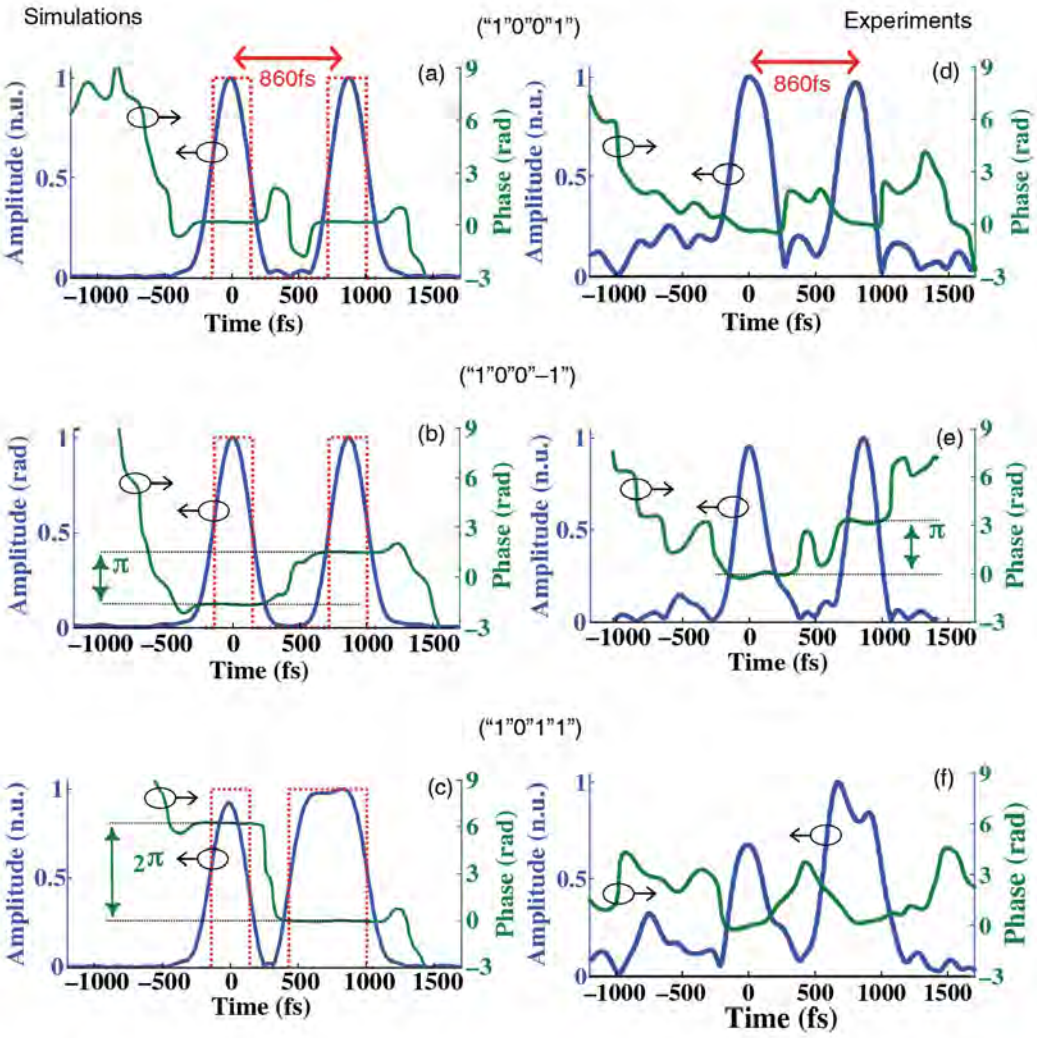

Figure 9.16 (a–c) Simulation results for the temporal amplitude (solid blue curves) and phase (solid green curves) responses of the designed LPGs to the OPO laser pulse data. The dotted, red curves in (a–c) represent the ideal time-domain impulse response amplitudes, obtained by using the predicted superluminal space-to-time scaling of the ideal space-domain profiles. (d–f) Measured output time-domain amplitude (solid blue curves) and phase (solid green curves) responses of the fabricated LPGs. *Source*: Ashrafi 2013 [101]. For a color version of this figure please see color plate section.

are shown in Figure 9.16 (d)–(f) in the color plate section. The responses of the LPGs are also simulated using the same grating design parameters and numerical simulation method used in the previous cases. The simulated spectral and temporal responses to the OPO laser pulse (numerically reconstructed from its spectrum data and assuming a linear spectral phase), are also presented in Figures 9.15 (d)–(f) and Figures 9.16 (a)–(c) respectively. There is a fairly good agreement between the numerically simulated and experimental results. Moreover, in the three reported examples, the obtained temporal responses at the system output closely follow the corresponding ideal impulse response that is predicted by the superluminal space-to-time mapping theory, both in amplitude

(ideal impulse responses represented with dotted, red curves) and in phase. The smoothing of the measured temporal responses with respect to the ideal impulse responses are due to the limited bandwidth of the input optical pulse.

Considering the superluminal space-to-time mapping value in the fabricated LPGs ($\backsim 833 \times 10^8$ m/s), the separation time of 860 fs between the first and last bits, shown in Figure 9.16, corresponds to a fairly large spatial length of ~7.12 cm, shown in Figures 9.15 (a)–(c). Thus, as anticipated, time resolutions in the femtosecond regime (e.g., for the inter-bit amplitude transitions and discrete phase jumps) can be achieved based on readily feasible sub-centimeter grating spatial resolutions.

In addition to optical pulse shapers based on LPGs, similar to FBG-based processing devices, recently two LPG-based signal processors, namely THz-bandwidth all-optical temporal differentiators and Hilbert transforms, have been realized and numerically demonstrated based on feasible fiber LPG designs [106, 107].

9.5 Advances towards Reconfigurable Schemes

As discussed in this chapter, one of the main limitations of fiber gratings solutions as pulse shapers is the lack of reconfigurability. However, several approaches can be considered in order to obtain reconfigurable pulse shapers based on this technology.

Fiber gratings can be employed as components in more complex configurations, where the programmability is achieved by controlling parameters unrelated with the gratings. For example, FBG-based optical differentiators have been suggested for their use in multi-arm configuration as optical pulse shapers [32]. In this approach, the desired (arbitrary) optical pulse shape is synthesized by coherently overlapping different successive time derivatives of an input optical pulse (not necessarily a Gaussian-shape pulse), including the input pulse itself, with suitable relative weights. Different output pulse shapes, e.g., rectangular, parabolic or triangular shapes, could be generated from the same platform by properly programming the relative weights among the different pulse derivatives. Strikingly, the effective bandwidth of the output pulse waveform is not necessarily limited by the input pulse bandwidth but rather it depends on the highest derivative order used for the pulse synthesis [32]. Also, FBG-based second order optical integrators have been recently used in a configuration denominated *time-delay to intensity mapping* [58]. A precise point-by-point control of the optical amplitude (intensity) of the waveform generated is achieved at the output of a second order optical integrator by simply tuning the input time-delay vector in an arrayed time-delay system. Using this approach, triangular, rectangular, and bright and dark parabolic pulses have been experimentally generated with temporal resolutions in the sub-picosecond regime. The performance of the pulse shaper is directly related with the number of taps employed in the circuit.

Programmable Bragg gratings have been proposed based on fiber and waveguide-based implementations [69, 108]. In fiber, reconfigurable coder/decoder for OCDMA applications have been implemented by using fine heating elements [69]. Still, the achieved performance needs to be improved to match the required standards for potential commercial purposes. In the case of integrated Bragg gratings, the designed devices use one-dimensional waveguide Bragg grating filled with an electrically controlled dielectric [108]. Arbitrary optical pulse shaping in the subhundred to a few hundred

picosecond regime has been theoretically proposed based on this technique, where the output pulses with desired shapes can be obtained by using a genetic algorithm providing the required voltages in each electrode.

Recently a wide range of tunable LPGs based on mechanically [109, 110], thermally [111], or electro-optically [112] controlled modulation of the refractive index along different waveguides/fibers has been reported. These technologies would potentially enable the implementation of the proposed femtosecond optical pulse shaping techniques based on LPGs in a programmable fashion. The development and implementation of such a programmable ultrafast optical pulse-shaping device would represent a significant advance in the field, and could potentially impact a very broad range of applications.

9.6 Conclusion

Fiber gratings are a stable and mature technology for the implementation of all-optical pulse shapers. They act as passive linear optical filters capable of reshaping any input pulse waveforms for optical signal processing, and are competent solutions whenever a fixed pulse shape is required, e.g., flat-top, parabolic, fixed complex modulated code, etc. Apart from their high degree of scalability and capacity of integration, fiber grating solutions offer an outstanding level of flexibility to implement any complex filter spectral response through variation of their physical characteristics, i.e., refractive index modulation or period profile. Recent advances in the design and implementation of fiber gratings have led to the achievement of operations bandwidths well in the THz regime, for both short and long period gratings. In the case of FBGs, a novel design technique for gratings operating in transmission has been introduced, allowing operation over broader frequency bandwidths without increasing the resolution and/or modulation depth in the grating apodization profile. Limitations in the implementation of minimum-phase-only functionalities have been overcome for the case of pulse processors operating over a limited time window. In the case of LPGs, a new design approach has been introduced, the so-called superluminal space-to-time mapping, that allows one to achieve ultrabroad operation bandwidths regardless of the resolution of the apodization profile in a straightforward manner. By employing these methods, a variety of optical pulse processors and shapers, with resolutions down to the sub-picosecond regime, have been numerically and experimentally demonstrated, including all-optical temporal differentiators, Hilbert transformers, flat-top, parabolic, triangular, and arbitrary code pulse shapers, etc. Advances toward reconfigurable schemes are being pursued nowadays through the use of innovative mechanisms to modify the grating physical features in a programmable fashion or by using fixed grating devices in more complex interferometric structures.

References

1 Lee, J.H., Oxenlowe, L.K., Ibsen, M., *et al.* (2003) All-optical TDM data demultiplexing at 80 Gb/s with significant timing jitter tolerance using a fiber Bragg grating based rectangular pulse switching technology. *Journal of Lightwave Technology*, **21** (11), 2518–2523.

2 Oxenlowe, L.K., Slavik, R., Galili, M., *et al.* (2008) 640 Gbit/s timing jitter tolerant data processing using a long-period fiber grating-based flat-top pulse shaper. *IEEE Journal of Selected Topics in Quantum Electronics*, **14**, 566–572.

3 Weiner, A.M., Silberberg, Y., Fouckhardt, H., *et al.* (1989) Use of femtosecond square pulses to avoid pulse breakup in all-optical switching. *IEEE Journal of Quantum Electronics*, **25** (12), 2648–2655.

4 Dutta, A.K., Dutta, N.K., and Fujiwara, M. (2004) *WDM Technologies: Optical Networks*, Elsevier Academic Press, New York.

5 Wabnitz, S. and Eggleton, B.J. (2015) *All-Optical Signal Processing: Data Communications and Storage Applications*, Springer, Berlin.

6 Iakushev, S.O., Shulika, O.V., Sukhoivanov, I.A., *et al.* (2014) Formation of ultrashort triangular pulses in optical fibers. *Optics Express*, **22** (23), 29 119–29 134.

7 Parmigiani, F., Petropoulos, P., Ibsen, M., and Richardson, D.J. (2006) Pulse retiming based on XPM using parabolic pulses formed in a fiber Bragg grating. *IEEE Photonics Technology Letters*, **18** (7), 829–832.

8 Ng, T.T., Parmigiani, F., Ibsen, M., *et al.* (2008) Compensation of linear distortions by using XPM with parabolic pulses as a time lens. *IEEE Photonics Technology Letters*, **20** (13), 1097–1099.

9 Parmigiani, F., Ibsen, M., Ng, T.T., *et al.* (2008) An efficient wavelength converter exploiting a grating-based saw-tooth pulse shaper. *IEEE Photonics Technology Letters*, **20** (17), 2008.

10 Schmogrow, R., Winter, M., Meyer, M., *et al.* (2012) Real-time Nyquist pulse generation beyond 100 Gbit/s and its relation to OFDM. *Optics Express*, **20** (1), 317–337.

11 Nakazawa, M., Hirooka, T., Ruan, P., and Guan, P. (2012) Ultrahigh-speed orthogonal TDM transmission with an optical Nyquist pulse train. *Optics Express*, **20** (2), 1129–1140.

12 Prucnal, P.R. (2006) *Optical Code Division Multiple Access: Fundamentals and Applications*, CRC Press, Boca Raton, FL.

13 Li, G.L. and Yu, P.K.L. (2003) Optical intensity modulators for digital and analog applications. *Journal of Lightwave Technology*, **19**, 2010–2030.

14 Dagli, N. (1999) Wide-bandwidth lasers and modulators for RF photonics. *IEEE Transactions on Microwave Theory and Techniques*, **47**, 1151–1171.

15 Weiner, A.M. (2011) Ultrafast optical pulse shaping: A tutorial review. *Optics Communications*, **284**, 3669–3692.

16 Weiner, A.M. (2000) Femtosecond pulse shaping using spatial light modulators. *Review of Scientific Instruments*, **71** (5), 1929–1960.

17 Cundiff, S.T., and Weiner, A.M. (2010) Optical arbitrary waveform generation. *Nature Photonics*, **4** (11), 760–766.

18 Saperstein, R.E., Panasenko, A.D., Roktiski, R., and Fainman, Y. (2005) Time-domain waveform processing by chromatic dispersion for temporal shaping of optical pulses. *Journal of the Optical Society of America B*, **22** (11), 2427–2436.

19 Kurokawa, T., Tsuda, H., Okamoto, K., *et al.* (1997) Time-space conversion optical signal processing using arrayed-waveguide grating. *Electronics Letters*, **33** (22), 1890–1891.

20 Muralidharan, B., Balakrishnan, V., and Weiner, A.M. (2006) Design of double-passed arrayed-waveguide gratings for the generation of flat-topped femtosecond pulse trains. *Journal of Lightwave Technology*, **24** (1), 586–597.

21 Fontaine, N.K., Geisler, D.J., Scott, R.P., He, T., Heritage, J.P., and Yoo, S.J.B. (2010) Demonstration of high-fidelity dynamic optical arbitrary waveform generation. *Optics Express*, **18**, 22 988–22 995.

22 Kolner, B.H. (1994) Space-time duality and the theory of temporal imaging. *IEEE Journal of Quantum Electronics*, **30** (8), 1951–1963.

23 Li, M., Han, Y., Pan, S., and Yao, J. (2001) Experimental demonstration of symmetrical waveform generation based on amplitude-only modulation in a fiber-based temporal pulse shaping system. *IEEE Photonics Technology Letters*, **23** (11), 715–717.

24 Chi, H. and Yao, J. (2007) Symmetrical waveform generation based on temporal pulse shaping using an amplitude-only modulator. *Electronics Letters*, **43** (7), 415–417.

25 Azana, J., Berger, N.K., Levit, B., and Fischer, B. (2005) Reconfigurable generation of high-repetition-rate optical pulse sequences based on time-domain phase-only filtering. *Optics Letters*, **30** (23), 3228–3230.

26 Wang, X. and Wada, N. (2007) Spectral phase encoding of ultra-short optical pulse in time domain for OCDMA application. *Optics Express*, **15** (12), 7319–7326.

27 Thomas, S., Malacarne, A., Fresi, F., *et al.* (2009) Programmable fiber-based picosecond optical pulse shaper using time-domain binary phase-only linear filtering. *Optics Letters*, **34** (4), 545–547.

28 Norberg, E.J., Guzzon, R.S., Nicholes, S.C., Parker, J.S., and Coldren, L.A. (2010) Programmable photonic lattice filters in InGaAsP-InP. *IEEE Photonics Technology Letters*, **22** (2), 109–111.

29 Dong, P., Feng, N.N., Feng, D., *et al.* (2010) Ghz-bandwidth optical filters based on high-order silicon ring resonators. *Optics Express*, **18**, 23 784–23 789.

30 Guan, B., Djordjevic, S.S., Fontaine, N.K., *et al.* (2014) CMOS compatible reconfigurable silicon photonic lattice filters using cascaded unit cells for RF-photonic processing. *IEEE Journal of Selected Topics in Quantum Electronics*, **20** (4), 8202 110.

31 Park, Y., Ashgari, M.H., Ahn, T.J., and Azana, J. (2007) Transform-limited picosecond pulse shaping based on temporal coherence synthesization. *Optics Express*, **15** (15), 9584–9599.

32 Asghari, M.H. and Azana, J. (2008) Proposal and analysis of a reconfigurable pulse shaping technique based on multi-arm optical differentiator. *Optics Communications*, **281**, 4581–4588.

33 Dudley, J.M., Finot, C., Millot, G., and Richardson, D.J. (2007) Self-similarity in ultrafast nonlinear optics. *Nature Physics*, **3** (9), 597–603.

34 Boscolo, S. and Finot, C. (2012) Nonlinear pulse shaping in fibres for pulse generation and optical processing. *International Journal of Optics*, **2012**, 1–14.

35 Erdogan, T. (1997) Fiber grating spectra. *Journal of Lightwave Technology*, **15** (8), 1277–1294.

36 Kashyap, R. (1999) *Fiber Bragg Gratings*, Academy Press, New York.

37 Miller, S.E. (1954) Coupled wave theory and waveguide applications. *Bell System Technical Journal*, **33**, 661–719.

38 Yariv, A. (1973) Coupled-mode theory for guided-wave optics. *IEEE Journal of Quantum Electronics*, **9**, 919–933.

39 Oppenheim, A.V. and Schafer, R.W. (1989) *Discrete-Time Signal Processing*, Prentice-Hall, New Jersey, 2nd edn.

40 Peral, E., Capmany, J., and Marti, J. (1996) Iterative solution to the Gel'Fand-Levitan-Marchenko coupled equations and application to synthesis of fiber gratings. *IEEE Journal of Quantum Electronics*, **32**, 2078–2084.

41 Feced, R., Zervas, M.N., and Muriel, M.A. (1999) An efficient inverse scattering algorithm for the design of non uniform fiber Bragg gratings. *IEEE Journal of Quantum Electronics*, **35**, 1105–1115.

42 Poladian, L. (2000) Simple grating synthesis algorithm. *Optics Letters*, **25**, 787–789.

43 Skaar, J., Wang, L., and Erdogan, T. (2001) On the synthesis of fiber Bragg gratings by layer peeling. *IEEE Journal of Quantum Electronics*, **37**, 165–173.

44 Kogelnik, H. (1976) Filter response of nonuniform almost-periodic structures. *Bell System Technical Journal*, **55**, 109–126.

45 Petropoulos, P., Ibsen, M., and Richardson, D.J. (2001) Rectangular pulse generation based on pulse reshaping using a superstructured fiber Bragg grating. *Journal of Lightwave Technology*, **19** (5), 746–752.

46 Parmigiani, F., Petropoulos, P., Ibsen, M., and Richardson, D.J. (2006) All-optical pulse reshaping and retiming systems incorporating pulse shaping fiber Bragg gratings. *Journal of Lightwave Technology*, **24** (1), 357–364.

47 Gatti, D., Fernandez, T.T., Longhi, S., and Laporta, P. (2010) Temporal differentiators based on highly-structured fibre Bragg gratings. *Electronics Letters*, **46**, 943–945.

48 Azana, J. and Chen, L.R. (2003) Synthesis of temporal optical waveforms by fiber Bragg gratings: a new approach based on space-to-time-to-frequency mapping. *Journal of the Optical Society of America B*, **19** (1), 2758–2769.

49 Berger, N.K., Levit, B., Fischer, B., *et al.* (2007) Temporal differentiation of optical signals using a phase-shifted fiber Bragg grating. *Optics Express*, **15** (2), 371–381.

50 Kulishov, M. and Azana, J. (2007) Design of high-order all-optical temporal differentiators based on multiple-phase-shifted fiber Bragg gratings. *Optics Express*, **15** (10), 6152–6166.

51 Rivas, L.M., Singh, K., Carballar, A., and Azana, J. (2007) Arbitrary-order ultrabroadband all-optical differentiators based on fiber Bragg gratings. *IEEE Photonics Technology Letters*, **19** (16), 1209–1211.

52 Li, M., Janner, D., Yao, J., and Pruneri, V. (2009) Arbitrary-order all-fiber temporal differentiator based on a fiber Bragg grating: design and experimental demonstration. *Optics Express*, **17** (22), 19 798–19 807.

53 Park, Y., Slavik, R., and Azana, J. (2007) Ultrafast all-optical differentiators for generation of orthogonal (sub-) picosecond Hermite-Gaussian waveforms, in *Optical Fiber Communication (OFC)*, OThI2.

54 Azana, J. (2008) Proposal of a uniform fiber Bragg grating as an ultrafast all-optical integrator. *Optics Letters*, **33** (1), 4–6.

55 Preciado, M.A. and Muriel, M.A. (2008) Ultrafast all-optical integrator based on a fiber Bragg grating: proposal and design. *Optics Letters*, **33** (12), 1348–1350.

56 Asghari, M.H. and Azana, J. (2008) Design of all-optical high-order temporal integrators based on multiple-phase-shifted Bragg gratings. *Optics Express*, **16** (15), 11 459–11 469.

57 Park, Y., Ahn, T.J., Dai, Y., Yao, J., and Azana, J. (2008) All-optical temporal integration of ultrafast pulse waveforms. *Optics Express*, **16** (22), 17 817–17 825.

58 Ashrafi, R., Dizaji, M.R., Romero Cortes, L., *et al.* (2015) Time-delay to intensity mapping based on a second-order optical integrator: application to optical arbitrary waveform generation. *Optics Express*, **23** (12), 16 209–16 223.

59 Slavik, R., Park, Y., Ayotte, N., *et al.* (2008) Photonic temporal integrator for all-optical computing. *Optics Express*, **16** (22), 18 202–18 214.

60 Asghari, M.H. and Azana, J. (2009) All-optical Hilbert transformer based on a single phase-shifted fiber Bragg grating: Design and analysis. *Optics Letters*, **34** (3), 334–336.

61 Cuadrado-Laborde, C. (2010) Proposal and design of a photonic in-fiber fractional Hilbert transformer. *IEEE Photonics Technology Letters*, **22** (1), 33–35.

62 Li, M. and Yao, J. (2010) All-fiber temporal photonic fractional Hilbert transformer based on a directly designed fiber Bragg grating. *Optics Letters*, **35** (2), 223–225.

63 Li, M. and Yao, J. (2010) Experimental demonstration of a wideband photonic temporal Hilbert transformer based on a single fiber Bragg grating. *IEEE Photonics Technology Letters*, **22** (21), 1559–1561.

64 Grunnet-Jepsen, A., Johnson, A.E., Maniloff, E.S., *et al.* (1999) Demonstration of all-fiber sparse lightwave CDMA based on temporal phase encoding. *IEEE Photonics Technology Letters*, **11**, 1283–1285.

65 Teh, P.C., Petropoulos, P., Ibsen, M., and Richardson, D.J. (2001) A comparative study of the performance of seven- and 63-chip otpical code-division multiple-access encoders and decoders based on superstructured fiber Bragg gratings. *Journal of Lightwave Technology*, **19** (9), 1352–1365.

66 Teh, P.C., Ibsen, M., Lee, J.H., Petropoulos, P., and Richardson, D.J. (2002) Demonstration of a four-channel WDM/OCDMA system using 255-chip 320-Gchip/s quarternary phase coding gratings. *IEEE Photonics Technology Letters*, **14**, 227–229.

67 Ayotte, S., Rochette, M., Magne, J., Rusch, L.A., and LaRochelle, S. (2005) Experimental verification and capacity prediction of FE-OCDMA using superimposed FBG. *Journal of Lightwave Technology*, **23** (2), 724–731.

68 Fang, X., Wang, D.N., and Li, S. (2003) Fiber Bragg grating for spectral phase optical code-division multiple-access encoding and decoding. *Journal of the Optical Society of America B*, **20**, 1603–1610.

69 Mokhtar, M.R., Ibsen, M., Teh, P.C., and Richardson, D.J. (2012) Simple dynamically reconfigurable OCDMA encoder/decoder based on uniform fiber Bragg grating, in *Optical Fiber Communications (OFC)*.

70 Chen, L.R. (2006) *Optical Code-Division Multiple Access Enabled by Fiber Bragg Grating Technology, in Optical CDMA: Fundamentals and Applications*, CRC Press, Boca Raton, FL.

71 Skaar, J. (2001) Synthesis of fiber Bragg gratings for use in transmission. *Journal of the Optical Society of America A*, **18** (3), 557–564.

72 Preciado, M.A. and Muriel, M.A. (2009) Flat-top pulse generation based on a fiber Bragg grating in transmission. *Optics Letters*, **34** (6), 752–754.

73 Preciado, M.A. and Muriel, M.A. (2008) Design of an ultrafast all-optical differentiator based on fiber Bragg grating in transmission. *Optics Letters*, **33** (21), 2458–2460.

74 Preciado, M.A., Shu, X., and Sugden, K. (2013) Proposal and design of phase-modulated fiber gratings in transmission for pulse shaping. *Optics Letters*, **38** (1), 70–72.

75 Slavik, R., Kulishov, M., Park, Y., and Azana, J. (2009) Long-period fiber-grating-based filter configuration enabling arbitrary linear filtering characteristics. *Optics Letters*, **34**, 1045–1047.

76 Kulishov, M., Krcmarik, D., and Slavik, R. (2007) Design of terahertz-bandwidth arbitrary-order temporal differentiators based on long-period fiber gratings. *Optics Letters*, **32**, 2978–2980.

77 Kim, S.J., Eom, T.J., Lee, B.H., and Park, C.S. (2003) Optical temporal encoding/decoding of short pulses using cascaded long-period fiber gratings. *Optics Express*, **11**, 3034–3040.

78 Park, Y., Kulishov, M., Slavik, R., and Azana, J. (2006) Picosecond and sub-picosecond flat-top pulse generation using uniform long-period fiber gratings. *Optics Express*, **14**, 12 670–12 678.

79 Slavik, R., Park, Y., Kulishov, M., and Azana, J. (2009) Terahertz-bandwidth high-order temporal differentiators based on phase-shifted long-period fiber gratings. *Optics Letters*, **34**, 3116–3118.

80 Strain, M.J. and Sorel, M. (2008) Integrated III-V Bragg gratings for arbitrary control over chirp and coupling coefficient. *IEEE Photonics Technology Letters*, **20** (22), 1863–1865.

81 Rivas, L.M., Strain, M.J., Duchesne, D., *et al.* (2008) Picosecond linear optical pulse shapers based on integrated waveguide Bragg gratings. *Optics Letters*, **33**, 2425–2427.

82 Strain, M.J. and Sorel, M. (2010) Desing and fabriction of integrated chirped Bragg gratings for on-chip dispersion control. *IEEE Journal of Quantum Electronics*, **46** (5), 774–782.

83 Burla, M., Romero Cortes, L., Li, M., *et al.* (2013) Integrated waveguide Bragg gratings for microwave photonics signal processing. *Optics Express*, **21** (21), 25 120–25 147.

84 Zhang, W., Li, W., and Yao, J. (2014) Optical differentiator based on integrated sidewall phase-shifted Bragg grating. *IEEE Photonics Technology Letters*, **26** (23), 2383–2386.

85 Burla, M., Li, M., Romero Cortes, L., *et al.* (2014) Terahertz-bandwidth photonic fractional Hilbert transformer based on a phase-shifted waveguide Bragg grating on silicon. *Optics Letters*, **39** (21), 6241–6244.

86 Simard, A.D., Strain, M.J., Meriggi, L., Sorel, M., and LaRochelle, S. (2015) Bandpass integrated Bragg gratings in silicon-on-insulator with well-controlled amplitude and phase responses. *Optics Letters*, **40** (5), 736–739.

87 Hinton, K. (1998) Dispersion compensation using apodized Bragg fiber gratings in transmission. *Journal of Lightwave Technology*, **16** (12), 2336–2347.

88 Poladian, L. (1997) Group-delay reconstruction for fiber Bragg gratings in reflection and transmission. *Optics Letters*, **22** (20), 1571–1573.

89 Fernandez-Ruiz, M.R., Carballar, A., and Azana, J. (2013) Design of ultrafast all-optical signal-processing devices based on fiber Bragg gratings in transmission. *Journal of Lightwave Technology*, **31** (10), 1593–1600.

90 Fernandez-Ruiz, M.R., Azana, J., and Carballar, A. (2012) Ultrafast all-optical Nth-order differentiators based on transmission fiber Bragg gratings, in *IEEE Photonics Conference (IPC)*, WCC3, pp. 656–657.

91 Fernandez-Ruiz, M.R., Li, M., *et al.* (2013) Picosecond optical signal processing based on transmissive fiber Bragg gratings. *Optics Letters*, **38** (7), 1247–1249.

92 Park, Y., Li, F., and Azana, J. (2006) Characterization and optimization of optical pulse differentiation using spectral interferometry. *IEEE Photonics Technology Letters*, **18** (17), 1798–1800.

93 Eggleton, J., Lenz, G., Slusher, R.E., and Litchinitser, N.M. (1998) Compression of optical pulses spectrally broadened by self-phase modulation using a fiber Bragg grating in transmission. *Applied Optics*, **37** (30), 7055–7061.

94 Fernandez-Ruiz, M.R., Carballar, A., and Azana, J. (2014) Arbitrary time-limited optical pulse processors based on transmission fiber Bragg gratings. *IEEE Photonics Technology Letters*, **26** (17), 1754–1757.

95 Ozcan, A., Digonnet, M.J.F., and Kino, G.S. (2006) Characterization of fiber Bragg gratings using spectral interferometry based on minimum-phase functions. *Journal of Lightwave Technology*, **24** (4), 1739–1757.

96 Carballar, A. and Janer, C. (2012) Complete fiber Bragg grating characterization using an alternative method based on spectral interferometry and minimum-phase reconstruction algorithms. *Journal of Lightwave Technology*, **30** (16), 2574–2582.

97 Fernandez-Ruiz, M.R., Wang, L., Carballar, A., *et al.* (2015) Thz-bandwidth photonic Hilbert transformers based on fiber Bragg gratings in transmission. *Optics Letters*, **40** (1), 41–44.

98 Slavik, R., Doucet, S., and LaRochelle, S. (2003) High-performance all-fiber Fabry-Perot filters with superimposed chirped Bragg gratings. *Journal of Lightwave Technology*, **21** (4), 1059–1065.

99 Ashrafi, R., Li, M., LaRochelle, S., and Azana, J. (2013) Superluminal space-to-time mapping in grating-assisted co-directional couplers. *Optics Express*, **21**, 6249–6256.

100 Ashrafi, R., Li, M., and Azana, J. (2013) Tsymbol/s optical coding based on long period gratings. *IEEE Photonics Technology Letters*, **25**, 910–913.

101 Ashrafi, R., Li, M., Belhadj, N., *et al.* (2013) Experimental demonstration of superluminal space-to-time mapping in long period gratings. *Optics Letters*, **38**, 1419–1421.

102 Jiang, J., Callender, C.L., Noad, J.P., and Ding, J. (2009) Hybrid silica/polymer long period gratings for wavelength filtering and power distribution. *Applied Optics*, **48**, 4866–4873.

103 Smietana, M., Bock, W.J., Mikulic, P., and Chen, J. (2011) Increasing sensitivity of arc-induced long-period gratings-pushing the fabrication technique toward its limits. *Measurement Science and Technology*, **22**, 015 201–1–015 201–6.

104 O'Regan, B.J. and Nikogosyan, D.N. (2011) Femtosecond UV long-period fibre grating fabrication with amplitude mask technique. *Optics Communications*, **284**, 5650–5654.

105 Lepetit, L., Cheriaux, G., and Joffre, M. (1995) Linear technique of phase measurement by femtosecond spectral interferometry for applications in spectroscopy. *Journal of the Optical Society of America B*, **12**, 2467–2474.

106 Ashrafi, R., Li, M., and Azana, J. (2013) Coupling-strength-independent long-period grating designs for Thz-bandwidth optical differentiators. *IEEE Photonics Journal*, **5**, 7100 311.

107 Ashrafi, R. and Azana, J. (2012) Terahertz bandwidth all-optical Hilbert transformers based on long-period gratings. *Optics Letters*, **37**, 2604–2606.

108 Wu, C. and Raymer, M.G. (2006) Efficient picosecond pulse shaping by programmable Bragg gratings. *IEEE Journal of Quantum Electronics*, **42** (9), 873–884.

109 Zhou, X., Shi, S., Zhang, Z., Zou, J., and Liu, Y. (2011) Mechanically-induced pi-shifted long-period fiber gratings. *Optics Express*, **19**, 6253–6259.

110 Chiang, C.C. (2010) Fabrication and characterization of sandwiched optical fibers with periodic gratings. *Applied Optics*, **49**, 4175–4181.

111 Jin, W., Chiang, K.S., and Liu, Q. (2010) Thermally tunable lithium-niobate long-period waveguide grating filter fabricated by reactive ion etching. *Optics Letters*, **35**, 484–486.

112 Balakrishnan, M., Spittel, R., Becker, M., *et al.* (2012) Polymer-filled silica fibers as a step towards electro-optically tunable fiber devices. *Journal of Lightwave Technology*, **30**, 1931–1936.